J. Mol. Biol. (1991) **218**, 233–260

Structural Mechanism for Glycogen Phosphorylase Control by Phosphorylation and AMP

D. Barford, S.-H. Hu and L. N. Johnson†

Laboratory of Molecular Biophysics
University of Oxford
Rex Richards Building
South Parks Road
Oxford, OX1 3QU, U.K.

(Received 23 July 1990; accepted 20 November 1990)

The crystal structures of activated R state glycogen phosphorylase *a* (GP*a*) and R and T state glycogen phosphorylase *b* (GP*b*) complexed with AMP have been solved at 2·9 Å, 2·9 Å and 2·2 Å resolution, respectively. The structure of R state GP*a* is nearly identical to the structure of sulphate-activated R state GP*b*, except in the region of Ser14, where there is a covalently attached phosphate group in GP*a* and a non-covalently attached sulphate group in GP*b*. The contacts made by the N-terminal tail residues in R state GP*a* at the subunit interface of the functionally active dimer are similar to those observed previously for T state GP*a*. The quaternary and tertiary structural changes on the T to R transition allow these interactions to be relayed to the catalytic site in R state GP*a*. The transition from the T state GP*b* structure to the R state GP*a* structure results in a change in the N-terminal residues from a poorly ordered extended structure that makes intrasubunit contacts to an ordered coiled conformation that makes intersubunit contacts. The distance between Arg10, the first residue to be located from the N terminus, in R state GP*a* and T state GP*b* is 50 Å. One of the important subunit–subunit interactions in the dimer molecule involves contacts between the helix α2 and the cap′ (residues 35′ to 45′ that form a loop between the 1st and 2nd α helices, α1′ and α2′ of the other subunit. The prime denotes residues from the other subunit). The interactions made by the N-terminal residues induce structural changes at the cap′/α2 helix interface that lead to the creation of a high-affinity AMP site. The tertiary structural changes at the cap (shifts 1·2 to 2·1 Å for residues 35 to 45) are partially compensated by the quaternary structural change so that the overall shifts in these residues after the combined tertiary and quaternary changes are between 0·5 and 1·3 Å. AMP binds to R state GP*b* with at least 100-fold greater affinity and exhibits four additional hydrogen bonds, stronger ionic interactions and more extensive van der Waals' interactions with 116 $Å^2$ greater solvent accessible surface area buried compared with AMP bound to T state GP*b*. A hydrogen bond observed in the R state complex between Asn44′ and the N-1 of the adenine moiety of AMP provides a possible explanation for the differences in affinity between AMP and IMP, and the different allosteric properties of the two nucleotides. The observed correlation between tertiary and quaternary conformational changes form the basis for a structural explanation for allosteric control by phosphorylation and by AMP.

1. Introduction

Glycogen phosphorylase was first shown to be dependent on AMP for activity by Cori *et al.* (1938). Later, detailed studies of this activation mechanism (Helmreich & Cori, 1964) were included as an important part of the body of evidence in the proposals for a unified mechanism of allosteric control (Monod *et al.*, 1965). Phosphorylase was the first enzyme recognized to be controlled by phosphorylation (Krebs & Fischer, 1956) and until the late 1960s this control mechanism was considered an idiosyncrasy of glycogen metabolism. Following the discoveries of cyclic-AMP-dependent protein kinase, and other protein kinases and phosphatases, it is now known that a large number of biological processes are regulated by phosphorylation events on serine, threonine or tyrosine residues (Krebs, 1986; Cohen, 1988; Yarden & Ullrich, 1988). These processes are as diverse as metabolism, muscle contractility, membrane transport, cell cycle control and protein

† Author to whom all correspondence should be addressed.

0022-2836/91/050233-28 $03.00/0

synthesis. In addition, prokaryote signal transduction is mediated through phosphorylation of aspartate and histidine residues (Stock *et al.*, 1990). Many of these enzymes are now understood in terms of their amino acid sequences and sites of phosphorylation but, to date, phosphorylase and isocitrate dehydrogenase (Hurley *et al.*, 1990*a*,*b*) are the only enzymes for which detailed structural data are available. This paper describes the conformational states of phosphorylase promoted by phosphorylation and AMP, and provides a structural basis for understanding the dual control properties in terms of allosteric mechanisms.

Glycogen phosphorylase (GP†) catalyses the intracellular degradation of glycogen into glucose 1-phosphate, the first step of glycolysis:

$$(\alpha\text{-1,4-glucoside})_n + P_i \leftrightarrow (\alpha\text{-1,4-glucoside})_{n-1} + \alpha\text{-glucose-1-P}.$$

The activity of the enzyme is regulated by the interconversion between alternative structural states, modulated by allosteric interactions and reversible phosphorylation. The T state exhibits a low level of affinity for substrates, whilst the R state exhibits a high level of affinity for substrates and allosteric activators. The non-phosphorylated form of the enzyme, phosphorylase *b* (GP*b*), is activated by micromolar concentrations of AMP. The enzyme displays homotropic co-operativity towards binding of substrates and AMP (Hill coefficient of 2 and 1·4, respectively (Buc, 1967; Black & Wang, 1968)) and heterotropic co-operativity between substrates and AMP (for example an increase in AMP concentration from 0·05 mM to 0·15 mM produces a 15-fold increase in affinity for phosphate (Helmreich & Cori, 1964)). The degree of homotropic co-operativity is dependent on the concentration of heterotropic effectors. Hormonal or neuronal signals stimulate kinase-catalysed phosphorylation of residue serine 14. The activity of the phosphorylated form, phosphorylase *a* (GP*a*) is independent of AMP. GP*a* binds substrates and AMP with a high level of affinity, although co-operatively. Activated GP*a* and GP*b* display comparable catalytic activities. The properties of phosphorylase have been reviewed (Graves & Wang, 1972; Madsen, 1986; Johnson *et al.*, 1989; Johnson & Barford, 1990).

In the absence of effectors, GP*b* is a dimer, each subunit has a relative molecular mass of 97,434. Activation by AMP or phosphorylation produces an association of dimers to form tetramers. Tetramers have 12 to 33% of the activity of the fully active dimers promoted by glycogen or oligosaccharide (Metzger *et al.*, 1967; Huang & Graves, 1970; Wang *et al.*, 1965). *In vivo*, phosphorylase is bound as the dimeric state to glycogen particles (Meyer *et al.*, 1970; Wanson & Drochmans, 1968; Busby & Radda, 1976).

Crystallographic investigations of various states of glycogen phosphorylase have provided insight into the mechanism of the co-operative behaviour on ligand binding and allosteric regulation. High-resolution structures are available for T state GP*b* crystallized with the weak activator IMP (Johnson *et al.*, 1974; Acharya *et al.*, 1990) and T state GP*a* crystallized in the presence of the inhibitor glucose (Fletterick *et al.*, 1976; Sprang & Fetterick, 1979). Comparison of these structures (Sprang *et al.*, 1988) showed that the predominant conformational changes associated with phosphorylation occur at the subunit interface as a result of a re-ordering of the N-terminal 20 residues. Communication of these changes to the catalytic site in T state GP*a* was prevented by glucose binding at the catalytic site. Crystals of R state GP were more difficult to obtain. The structure of R state GP*b* crystallized from 1·0 M-ammonium sulphate has been determined at 2·9 Å (1 Å = 0·1 nm) resolution (Barford & Johnson, 1989), and has provided a structural basis for understanding the T to R transition in terms of tertiary and quaternary structural changes. Sulphate mimics phosphoserine at the Ser-P site and phosphate groups at the catalytic and allosteric sites. High concentrations of sulphate induce the R state characteristics of GP. In the presence of 0·9 M-ammonium sulphate, the activity of the enzyme reaches 50% of the level of GP*a* or AMP-activated GP*b*, concomitant with an increased affinity for glycogen equivalent to that for GP*a*. Sulphate stimulates AMP-induced activation of GP*b* through a 50-fold increase in affinity of the enzyme for AMP and abolition of homotropic co-operativity on AMP binding (Engers & Madsen, 1968; Sotiroudis *et al.*, 1978; Leonidas *et al.*, 1990). A reduced affinity for Glc 1-P (Leonidas *et al.*, 1990) most likely arises from competitive inhibition by sulphate, which binds to the catalytic site.

The subunit structure of GP is representative of the α/β class of proteins with the polypeptide chain folded into two domains, the N-terminal domain consists of residues 1 to 484 with the C-terminal domain consisting of residues 485 to 842. A detailed description of the structure of T state GP*b* refined at a resolution of 1·9 Å to an *R*-factor of 19% has been reported (Acharya *et al.*, 1990). Two subunits of the functional dimer associate at two positions located on opposite sides of the enzyme molecule (Fig. 1). One contact, the cap′/α2 interface is formed by the association of the cap′ (residues 35′ to 46′), a loop connecting the α1′ and α2′ helices, with the β7 strand (residues 191 to 193) and α2 helix (residues 47 to 78) of the other subunit. (Residues from the symmetry-related molecule are denoted by the prime.) This interface includes the allosteric effector site and Ser-P binding site (Fig. 1(a) and (b)). An identical interface is produced by the molecular

† Abbreviations used: GP*a* and GP*b*, glycogen phosphorylase *a* and glycogen phosphorylase *b*; r.m.s., root-mean-square; R_m, merging *R* is defined as $R_m = \Sigma_h\Sigma_i|I(h) - I_i(h)|/\Sigma_h\Sigma_i I_i(h)$, where $I_i(h)$ and $I(h)$ are the *i*th and the mean measurement of the intensity of reflection *h*, respectively; BES, 2-(bis(2-hydroxyethyl)amino)ethane sulphonic acid; NCS, non-crystallographic symmetry.

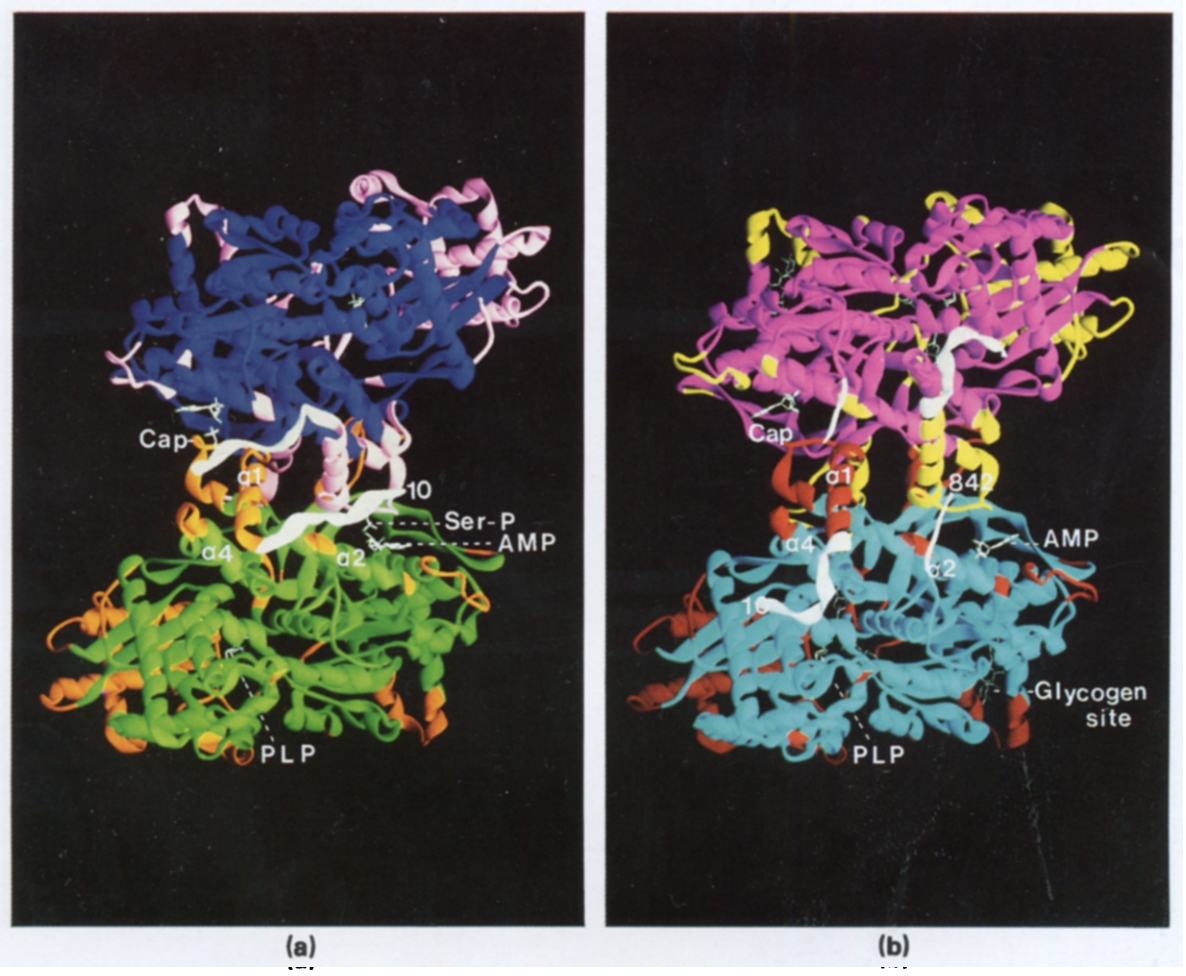

Figure 1. R state GP*a* and T state GP*b* dimers. Colour code: (a), (c) and (e) R state subunit 1 green and subunit 2 blue with regions that differ by more than 1 Å in C^{α} positions between R and T state tertiary structures shown in orange and pink for subunits 1 and 2, respectively; (b), (d) and (f) T state subunit 1 cyan and subunit 2 purple with regions that differ more than 1 Å in C^{α} positions between R and T states shown in red and yellow. The N-terminal residues (10 to 23) and the C-terminal residues (837 to 842) are shown in white. Ligands: pyridoxal phosphate and sulphate (R state) and glucose 1-P (T state) are shown at the catalytic site; AMP at the allosteric effector site; Ser-P at Ser14 (R state GP*a* only); AMP at the nucleoside inhibitor site (T state only); and maltopentose at the glycogen storage site (T state only). (a) and (b) A view down the 2-fold axis of the dimer with the allosteric sites and Ser-P sites towards the viewer. The catalytic site is at the rear. The view shows the change in conformation of the N-terminal tail from intra to inter-subunit contacts and the shifts of the α1 helix–cap–α2 helix and α4–α5 inter-helix loop. (c) and (d) A view down the 2-fold axis of the dimer with the catalytic site and tower helices towards the viewer. The allosteric site is at the rear. The view illustrates the changes in the tower helices and the 280s loop. The shifts in the helix bundle (lower right; orange and red in R and T states) are part of the dimer–dimer contact in the tetramer in which these helices pack against part of the glycogen storage site (left). (e) and (f) A view normal to the 2-fold axis of the dimer. The view shows the change in quaternary structure in which one subunit (subunit 2; top) rotates 10° with respect to the other (subunit 1; bottom) about an axis normal to the 2-fold axis that intercepts the axis at a point near the cap′/α2 interface. The view shows changes at the subunit–subunit interface and the shifts of the N-terminal and C-terminal residues. Ribbon diagram by Carson & Bugg (1986).

2-fold symmetry operation. A second subunit–subunit contact involves the tower interface and consists of the antiparallel association of two symmetry-related helices, α7 (residues 262 to 276), that link the subunit interface with the catalytic site (Fig. 1(c) and (d)). The catalytic site, buried 15 Å below the molecular surface, is located at the interface of the two domains, adjacent to the essential cofactor pyridoxal 5′-phosphate. Access to this site is achieved through a tunnel, which in the T state is restricted mostly by the 280s loop (residues 282 to 286). The residues from the 280s loop are displaced on transition to the R state following motion of the tower helices (Barford & Johnson, 1989). A concerted motion of Asp283 and Arg569 creates a high-affinity phosphate-binding site adjacent to the cofactor. An inhibitor site in T state GP is located at the entrance to the catalytic site tunnel, formed from the side-chains of Phe285 and Tyr613. Non-specific binding of nucleosides and nucleotides at this site act in synergism with glucose at the catalytic site to stabilize the T state conformation of the 280s loop (Kasvinsky *et al.*, 1978: and see Fig. 1(c) and (d)). In the R state, displacement

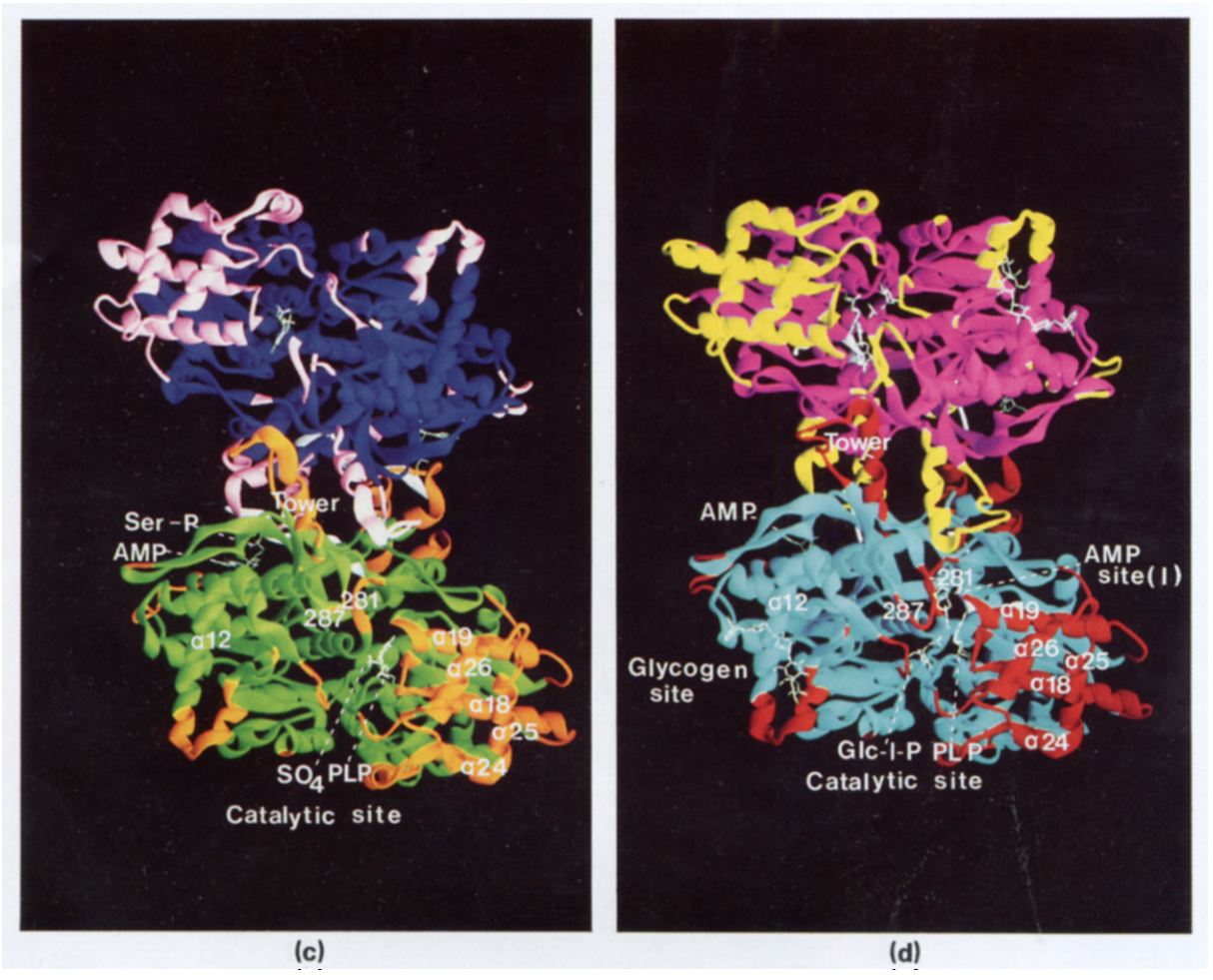

Fig. 1.

of the 280s loop prevents inhibition due to nucleosides and glucose. The catalytic site is separated from the allosteric site and Ser-P site by 35 Å and 45 Å, respectively, and from the symmetry-related catalytic site by 70 Å. The Ser-P site is located 15 Å from the allosteric site and symmetry-related allosteric and Ser-P sites are separated by 40 Å and 35 Å, respectively. Long-range interactions therefore operate between different ligand-binding sites.

Here, we describe the structure of the R state of GP*a* and the structures of AMP bound to the R state and T state of GP*b*. It is shown that protein phosphorylation and ligation of the allosteric effector AMP stabilize the R state quaternary conformation by promoting the R state conformation at the cap′/α2 interface, similarly to that observed previously in T state GP*a* and in sulphate-activated GP*b*.

2. Methods

Rabbit skeletal muscle phosphorylase *b* was prepared following the procedure of Fischer & Krebs (1962). Phosphorylase *b* was converted to phosphorylase *a* through phosphorylase kinase-catalysed phosphorylation of serine 14. Chemicals and phosphorylase kinase were purchased from either Sigma or BDH. R state GP*a* and GP*b* crystallize in the monoclinic form (space group $P2_1$, $a=119{\cdot}0$ Å, $b=190{\cdot}0$ Å, $c=88{\cdot}2$ Å, $\beta=109{\cdot}35°$; 1 tetramer of 390,000 M_r/asymmetric unit) in the presence of 1·0 M-ammonium sulphate, 10 mM-β-glycerophosphate (pH 7·5) as described by Madsen *et al.* (1972) and Fasold *et al.* (1972). T state GP*b* tetragonal crystals (space group $P4_32_12$, $a=b=128{\cdot}5$ Å; $c=116{\cdot}3$ Å, 1 subunit/asymmetric unit, with the symmetry-related molecule produced by the crystallographic 2-fold at $z=1/2$) were grown in the presence of 2 mM-IMP and 10 mM-magnesium acetate by the method of Johnson *et al.* (1974).

(a) *Monoclinic crystals: R state phosphorylase* a *and R state phosphorylase* b–*AMP complex*

Crystals of R state GP*b*–AMP complex were prepared by soaking native GP*b* crystals in a solution containing 100 mM-AMP, 10 mM-β-glycerophosphate, 1·0 M-ammonium sulphate (pH 7·5) for 12 h before mounting. Three-dimensional 2·9 Å resolution data sets were collected for native GP*a* and the R state GP*b*–AMP complex on an Arndt–Wonacott oscillation camera (Arndt & Wonacott, 1977) mounted on the Wiggler beam line PX 9·6 at the SRS Daresbury. Crystals were aligned with a^* coincident with the crystal rotation axis and data recorded on contiguous packs with a spindle oscillation range of 1°/film pack. In all, 90 packs corresponding to a rotation range of 90° were recorded. The wavelength was

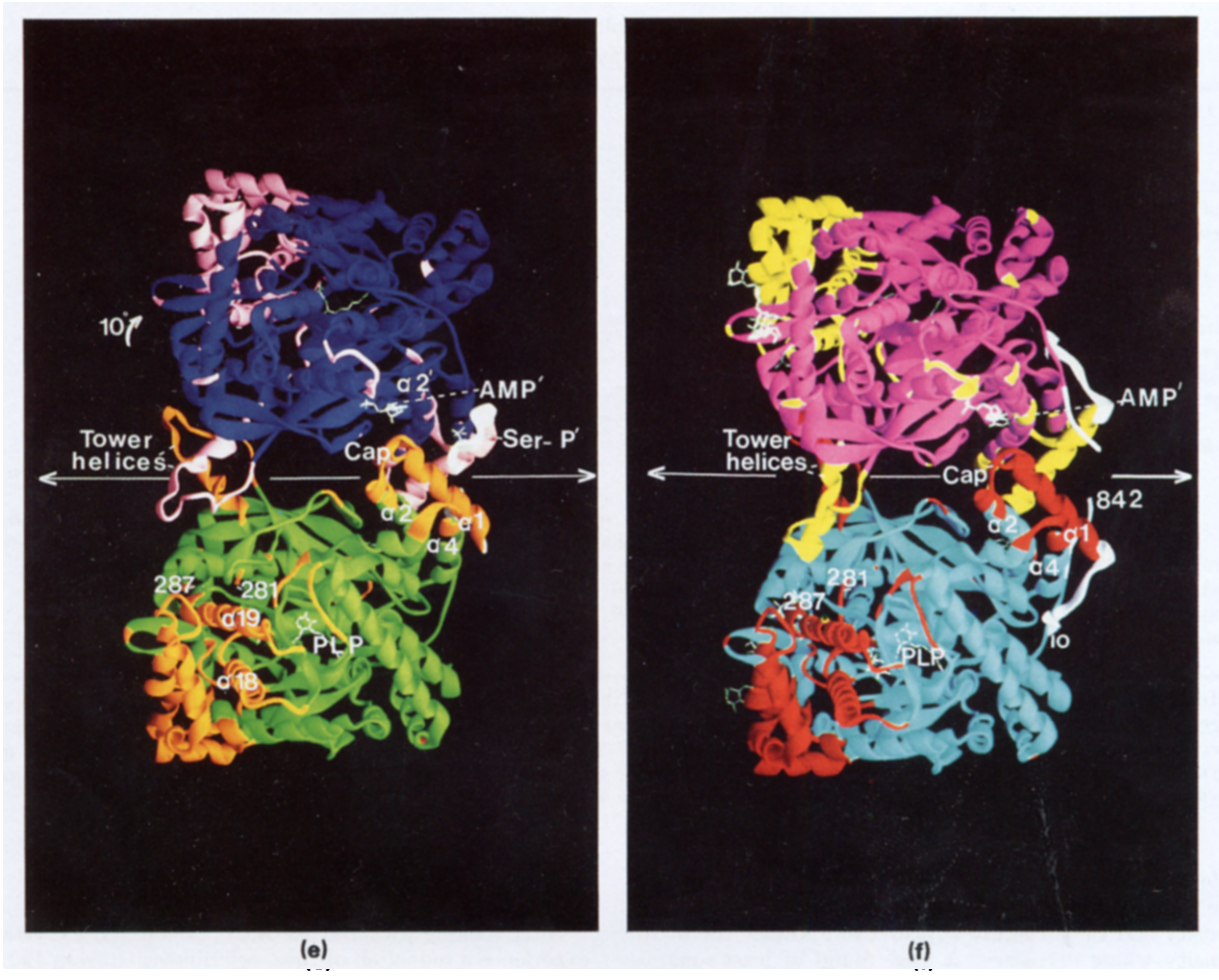

Fig. 1.

0·88 Å and the synchrotron was operated at 2·0 GeV with current ranging from 250 to 150 mA.

Crystal orientations were determined using the auto-indexing routine REFIX of Kabsch (1988). Films were scanned on a Joyce–Loebl Scandig 3 microdensitometer and the intensities integrated by profile fitting with a modified version (D. I. Stuart) of the MOSCO data-processing program (Nybourg & Wonacott, 1977). Intra-film pack scaling and application of corrections for oblique incidence and Lorentz polarization were performed by ABSCALE (CCP4 program suite, Daresbury Laboratory, U.K.). Interpack scaling, partial reflection summation and data reduction were performed by AGROVATA and ROTAVATA (CCP4). Data processing statistics are summarized in Table 1. Data were scaled to the native R state GP*b* amplitudes using an anisotropic scaling procedure (ANISOSC, CCP4) and to structure factor amplitudes calculated from the refined model using a shell scaling method (D. I. Stuart, unpublished results). The mean fractional isomorphous difference in amplitudes was 11% between R state GP*b* and GP*a*, and 20% between R state GP*b* and the GP*b*–AMP complex.

(i) *Refinement of R state GPa*

An electron density map was calculated using coefficients $(2Fo_{GPa} - Fc_{GPb})$ and α_{GPb}, where Fo_{GPa} are observed amplitudes for GP*a*, and Fc_{GPb} and α_{GPb} are the amplitudes and phases calculated from the refined model of GP*b*. The map showed continuous density bridging C^{β} of serine 14 and a phosphate group, indicative of a covalent attachment between the serine and phosphate groups (Fig. 2(a)). In R state GP*b*, the Ser-P group is mimicked by the non-covalent association of a sulphate ion, and there is a break in the electron density between the serine side-chain and the anion (Fig. 2(b)). Initial co-ordinates used in refinement were those of the refined structure of R-state GP*b* modified for a Ser-P group at residue 14. The energy parameters for the Ser-P group were based on serine and phosphate parameters. Refinement employing the X-PLOR program (Brunger, 1989; Brunger *et al.*, 1989) proceeded for a tetramer of 4 equivalent subunits with the application of tight non-crystallographic symmetry (NCS) restraints (100 kcal mol^{-1}: 1 cal = 4·184 J), which function to maintain molecular equivalence and increase the ratio of observations to parameters, as described by Weiss *et al.* (1990). The 1st stage of refinement consisted of 150 cycles of least-squares atomic positional refinement, which resulted in a drop in *R*-factor from the initial 36·5% to 27·0%. In the 2nd stage, simulated annealing performing molecular dynamics for a duration of 0·5 ps at 4000 K (heatstage), followed by a coolstage consisting of dynamics simulation at 300 K for 0·25 ps, reduced the *R*-factor to 25·7%. Further least-squares positional refinement with gradual reduction of the non-crystallographic energy restraints reduced the *R*-factor to 20·2%. After atomic *B*-factor refinement, the *R*-factor was 18·2%. At this stage, a $2F_o - F_c$ map was calculated using F_c values and phases

Table 1

Crystal parameters, data processing and refinement of GPa and GPb–AMP complexes

A. *Crystal parameters*

	Space group	a	b (unit cell Å)	c	β (deg.)
R state GP*a*	$P2_1$	119·0	190·0	88·2	109·35
R state GP*b*/AMP	$P2_1$	119·0	189·0	88·2	109·2
T state GP*b*/AMP	$P4_32_12$	128·5	128·5	116·3	

B. *Data processing statistics*

Data set	No of crystals	No. reflections measured	No. unique reflections	R_m	% complete (resolution, Å)
R state GP*a*	8	118,156	67,048	0·094	93 (2·9)
R state GP*b*/AMP	6	107,979	64,048	0·115	89 (2·9)
T state GP*b*/AMP	1	165,007	36,295	0·080	80 (2·2)

C. *Refinement parameters*

			No. of Ligand atoms				r.m.s. deviation from ideal	
Structure	Reflections $F>\sigma_F$	No. of protein atoms	No. of sulphate atoms	No. of AMP atoms	No. of water molecules	R-factor	Bond length (Å)	Bond angles (deg.)
R state GP*a*	61,486	26,994	40	—	—	0·176	0·020	4·2
R state GP*b*/AMP	58,103	26,382	40	92	—	0·171	0·018	3·6
T state GP*b*/AMP	36,167	6787		46	640	0·206	0·018	3·6

In R state GP*a*, sulphate binds at the allosteric (AMP) site and the catalytic site in all 4 subunits of the asymmetric unit. There are therefore 40 sulphate atoms. In R state GP*b*–AMP complex, sulphate binds at the Ser-P and catalytic sites in all 4 subunits and hence there are 40 sulphate atoms. AMP is bound at the allosteric sites of the 4 subunits and hence there are 4×23 AMP atoms per asymmetric unit. In T state GP*b*–AMP complex, AMP binds to the allosteric site and the inhibitor site, and there is only 1 subunit per asymmetric unit. Hence, there are 46 AMP atoms per asymmetric unit.

calculated from the refined model, and the structure of the entire tetramer was inspected against the electron density and the structure adjusted to optimize the fit to density where necessary. A final round of least-squares positional and B-factor refinement brought the R-factor to 17·6% with reasonable stereochemistry (Table 1).

A plot of temperature factor for main-chain atoms *versus* residue number is shown in Fig. 3(a) for R state GP*a* subunit 1. The other subunits show similar plots and these are also close to those obtained for R state GP*b* (not shown). The average B-factors for the main-chain atoms for subunits 1, 2, 3 and 4 were 22·2, 23·4, 22·9 and 25·9 Å^2, respectively. Residues whose average main-chain B-factors exceeded 44 Å^2 are indicated in Fig. 3(a). These residues indicate parts of the structure that are poorly determined. A Ramachandran plot for subunit 1 is shown in Fig. 3(c). Most of the residues have dihedral angles that conform to the allowed regions defined by potential energy calculations (e.g. see Schulz & Schirmer, 1979). Each subunit gave a similar Ramachandran plot and there were 16, 15, 19 and 16 non-glycine residues for subunits 1, 2, 3 and 4, respectively, that showed dihedral angles that differed by more than 15° from the allowed regions. (These are indicated for subunit 1 in Fig. 3(c).) Several of these residues are from parts of the structure that are ill determined, and exhibit poor electron density and high temperature factors. These regions include residues 19 to 21, 252 to 258, 314 to 320, 553 to 556 and 835–836. Other residues appeared to be in satisfactory electron density with no obvious scope for improvement but were on the edge of the allowed regions in the Ramachandran plot, so that a small change in positional parameters could result in angles that conformed to accepted values. These residues, which probably contain positional errors, include Asp78, Ala103, Phe166, Tyr233, Arg358, Val436, Ala610, Ser674, Asn678 and Glu730 for subunit 1. All of these, except Asn678, are on surface loops.

(ii) *Refinement of R state GP*b*–AMP complex*

After soaking with 100 mM-AMP, R state GP*b* crystals experience a reduction of the b-cell dimension from 190 Å to 189 Å. Non-isomorphism is evident after scaling native GP*b* amplitudes to the derivative (AMP complex) amplitudes, producing a mean fractional isomorphous change of 20% with the fractional isomorphous change steeply increasing as a function of resolution to 47% at 2·9 Å. A map obtained using coefficients ($Fo_{AMP}-Fo_{GPb}$) and α_{GPb}, where α_{GPb} are phases calculated from the refined GP*b* model, was noisy and not easily interpretable.

Further to this, a difference Fourier electron density map was calculated using coefficients ($Fo_{AMP}-Fc_{GPb}$) and α_{GPb}, with Fo_{AMP} and Fc_{GPb} weighted according to Rayment (1983). The map was averaged over the 4 copies of the subunit according to their geometric relationship. Well-resolved density corresponding to AMP located at the allosteric site was observed as the highest feature, allowing the position and conformation of the nucleotide to be determined (Fig. 4(a)). The starting model for refinement was based on the refined GP*b* R-state co-ordinates and the AMP molecule fitted with a 2′ *endo* ribose pucker (i.e. similar to that observed for AMP binding to T state GP*a* (Sprang *et al.*, 1987)). The AMP was fitted to the averaged density map and transformed to the allosteric sites of the other 3 subunits. A negative peak over the side-chain of Tyr75 and an associated positive peak indicated a motion of this residue towards the nucleotide. The model was subjected to 250 cycles of least-squares conjugent gradient refinement with non-crystallographic symmetry (NCS) restraints of 200 kcal mol^{-1} applied, reducing the R-factor from the initial 29·9% to 26·2%. Further atomic positional refinement with gradual reduction of the NCS restraints reduced the R-factor to 19·1% which, following atomic B-factor refinement, converged at 18·0%. At this stage a density map calculated using

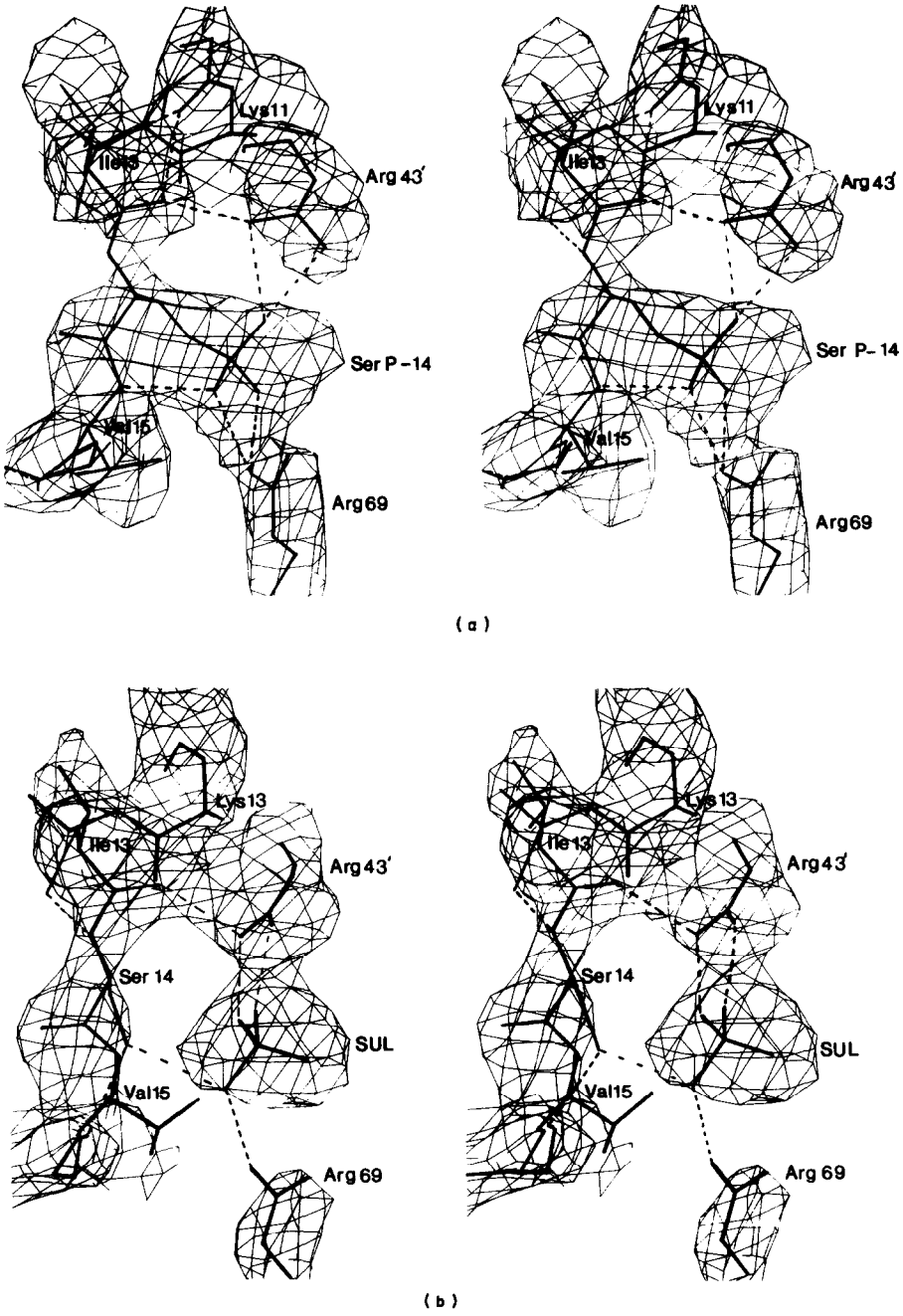

Figure 2. Stereo views of the electron density in the vicinity of Ser14 for (a) R state GP*a* showing the covalent attachment of phosphate and (b) R state GP*b* showing non-covalent association of sulphate. The side-chains of Arg69, Arg43′ and Val15 are included. Both maps are based on coefficients $2F_o - F_c$ and α_{calc} after the respective refinements and contoured at 0·9 arbitrary units (approx. 1 r.m.s. deviation of the map).

coefficients ($2Fo_{AMP} - Fc_{AMP}$) and α_{AMP} was inspected and revealed improved density at the allosteric site. The electron density corresponding to ribose showed clear indications for the position of the ribose 2′ and 3′ hydroxyl groups and was more consistent with AMP adopting the 3′ *endo* rather than the 2′ *endo* conformation. The single crystal structure of 3′ *endo* AMP reported by Kraut & Jensen (1963) was fitted to the density, with only minor torsion angle adjustments, indicating that AMP is bound to the enzyme in a conformation similar to that found in the solid state. Energy parameters for the AMP molecule were based on the nucleic acid parameters provided in X-PLOR. Additional refinement was performed before the entire model was inspected against a $2F_o - F_c$ map. Manual adjustments of the model were made where necessary, and a final round of 100 cycles of atomic positional and *B*-factor refinement reduced the *R*-factor to 17·1% (Table 1). The final structure exhibited acceptable stereochemistry, with the r.m.s. deviation of C^{α}-atoms of all subunits from the mean of 0·3 Å. The average *B*-factors for main-chain atoms were 28·3, 33·2, 31·5 and 34·9 Å^2 for subunits 1, 2, 3 and 4, respectively, and are slightly higher than those obtained for R state GP*a* (Fig. 3(a)), possibly because of the perturbation of the crystal lattice that results in a decreased cell dimension. Ramachandran plots of the individual subunits (not shown) had similar features to those noted for the R state GP*a* structure.

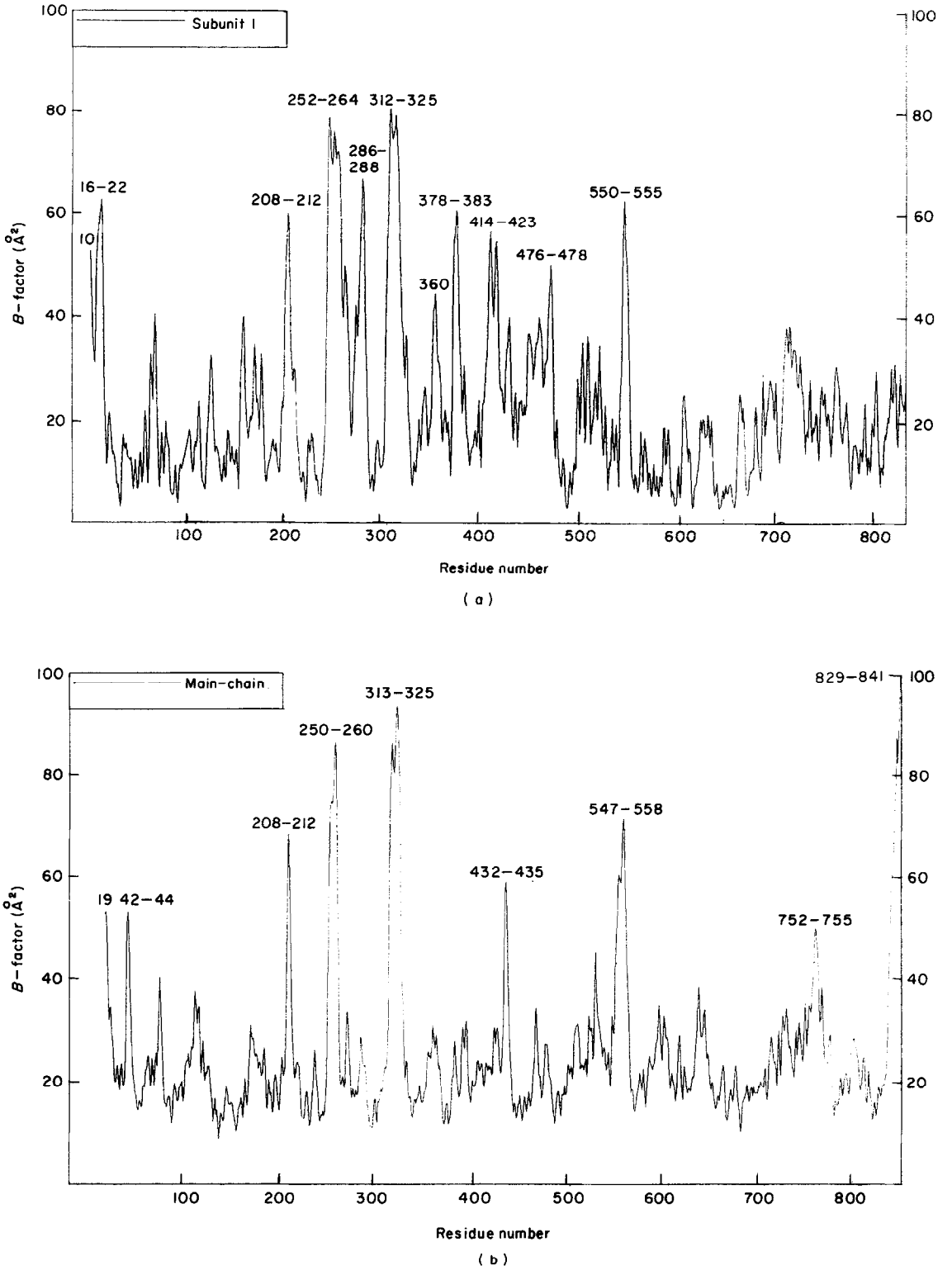

Figure 3. (a) Plot of average *B*-factors for main-chain atoms *versus* residue number for R state GP*a* subunit 1. The average *B*-factor for all main-chain atoms is 22·2 Å^2. Residues with *B*-factors greater than 44 Å^2 are labelled. (b) Plot of average *B*-factors for the main-chain atoms *versus* residue number for T state GP*b*–AMP complex. The average *B*-factor for all main-chain atoms is 25·4 Å^2. Residues whose *B*-factors exceed 44 Å^2 are labelled. (c) A Ramachandran plot for R state GP*a* subunit 1. The boundaries of the allowed regions using a hard sphere model are shown. The non-glycine residues whose dihedral angles differ by more than 15° from the allowed potential energy values are numbered. (*) Pro; (×) Gly; (+) others. (d) A Ramachandran plot for T state GP*b*–AMP complex. The diagram is labelled as for (c).

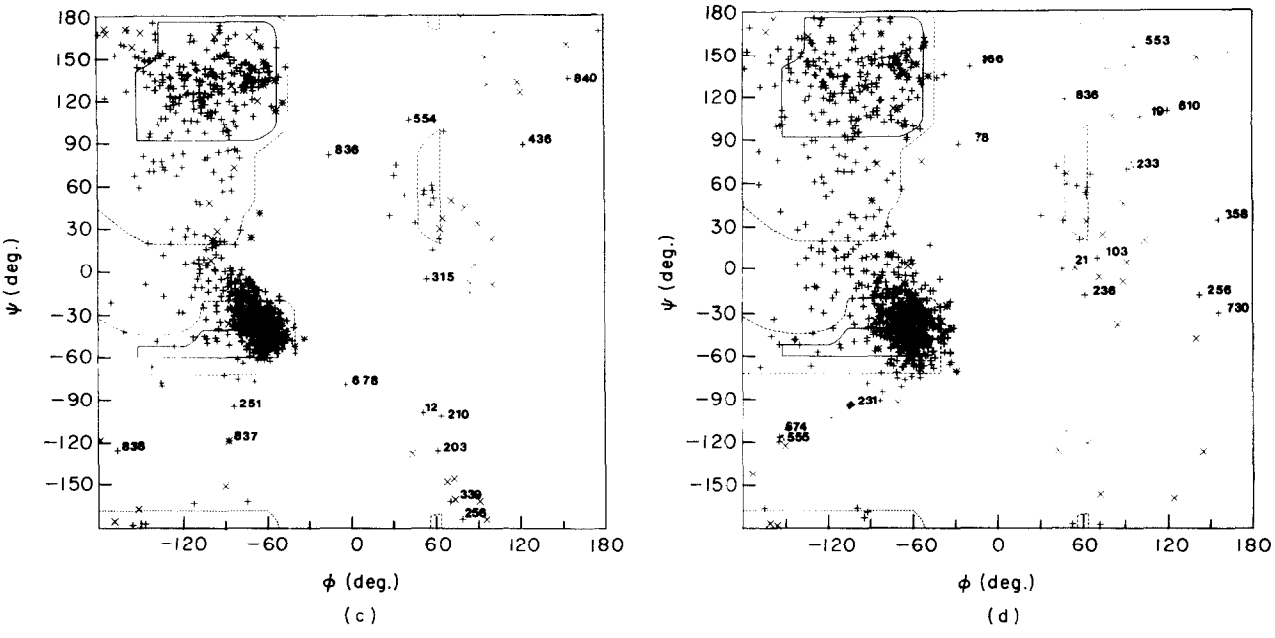

Fig. 3.

(b) *Tetragonal crystals: T state phosphorylase b–AMP complex*

T state GP*b* tetragonal crystals were soaked in a solution of 100 mM-AMP, 100 mM-BES, 10 mM-magnesium acetate (pH 6·7) for 12 h before mounting in a thin-walled glass capillary tube. Data to a resolution of 2·2 Å were collected on a Xentronics electronics area detector operating on a Rigaku rotating anode generator with current of 60 mA, voltage 50 kV, producing CuKα X-radiation of wavelength 1·54 Å. Two ϕ settings for the crystal, separated by 30°, were used with the ω axis rotated through 90° and data recorded on 460 contiguous frames of 0·2° oscillation.

Processing of images collected on the Xentronics area detector was performed using the XENGEN program package (Howard *et al.*, 1987). Crystal orientation, camera and crystal parameters were determined with an auto-indexing routine and refined. The refined unit cell dimensions are identical to those of native crystals. Reflection intensities were determined and data reduced and scaled, and final statistics are given in Table 1. The method of French & Wilson (1978) was used in order to correct for negative intensities with the CCP4 program TRUNCATE. Structure factor amplitudes were combined and scaled against a 2·2 Å resolution native data set previously collected on the Xentronics area detector (J. L. Martin, unpublished results) using CADLCF and ANISOSC (CCP4). The mean fractional isomorphous difference between native and derivative data is 11·4%. A difference Fourier map (Fig. 4(b)) was calculated using coefficients $m(F_{AMP} - F_{nat})$ and α_{nat}, where F_{nat} and F_{AMP} are the native and derivative structure factor amplitudes, respectively, m is the figure of merit associated with the phase, α_{nat}, calculated from the refined 1·9 Å T state phosphorylase *b* model (Acharya *et al.*, 1990). The map was inspected against the GP*b* model and AMP co-ordinates from the single crystal structure determination reported by Kraut & Jensen (1963) were fitted to the positive electron density at the allosteric and inhibitor sites. The structure of the density at the ribose sub-site at the allosteric site indicated a 3′ *endo* conformation of the sugar. The conformation about the glycosidic bond is *anti*. A negative electron density peak corresponding to the side-chain of Arg309 and associated positive peak indicated a new position for this side-chain and torsion angles were adjusted accordingly. Small positive peaks were observed overlying the positions of Arg310 and Gln71 side-chains, suggesting that these side-chains are less mobile in the presence of AMP. Weak negative density was observed in the region of the side-chains of Asp42′ and Val45′ of the cap′, indicating a displacement or disordering of the cap′. Five water molecules at the allosteric site and 6 at the inhibitor site are displaced on ligation of AMP and these were deleted from the protein co-ordinate file.

(i) *Refinement of T state GP*b*–AMP complex*

The starting model for refinement was the 1·9 Å refined GP*b* structure (residues 10 to 842) with water molecules and AMP fitted to the allosteric and inhibitor sites. Subjecting this model to 200 steps of least-squares conjugent gradient refinement employing X-PLOR reduced the *R*-factor from 28·9% to 24·9%. A simulated annealing cycle was performed consisting of 1000 molecular dynamic steps of duration 0·5 fs at 4000 K and 350 steps of 0·1 fs at 300 K. This brought the *R*-factor to 25·7%. Harmonic constraints of 300 kcal mol^{-1} were imposed on the water molecule co-ordinates to prevent excessive motion during the high-temperature dynamics simulation. Further least-squares positional and *B*-factor refinement reduced the *R*-factor to 20·6%. Statistics are presented in Table 1.

The refined position of AMP is well supported in the electron density map obtained using coefficients $2F_o - F_c$ with phases calculated from the refined model. Density corresponding to the phosphate and ribose groups is strong, with slightly weaker density occurring for adenine.

The average *B*-factor for main-chain atoms was 25·4 $Å^2$, and a plot of *B*-factor *versus* residue number is shown in Fig. 3(b). The regions that are poorly ordered with *B*-factors greater than 44 $Å^2$ are indicated. The

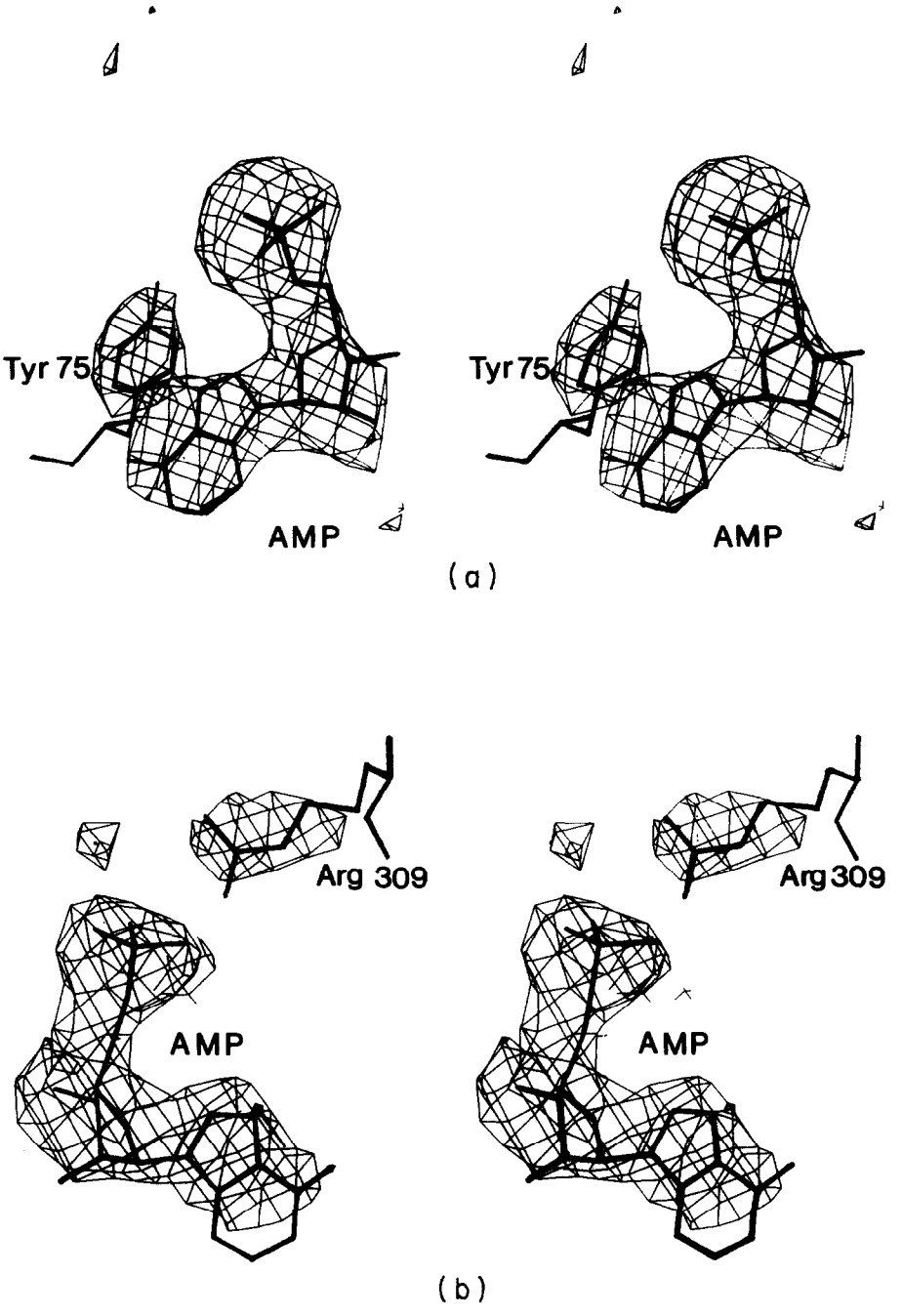

Figure 4. Stereo views of the difference electron density maps for AMP bound to (a) R state GP*b* and (b) T state GP*b*. Different views are shown in order to illustrate the fit of the nucleotide to the density. The coefficients are: for R state $Fo_{AMP}-Fc_{GPb}$ and α_{GPb} with Rayment (1983) weights and electron density averaged over the 4 subunits; for T state, the coefficients were $F_{AMP}-F_{nat}$ and α_{nat}. For further details, see the text.

Ramachandran plot for T state GP*b*–AMP complex is shown in Fig. 3(d). There are 14 residues whose dihedral angles differ by more than 15° from the allowed values. These include residues from the regions of the molecule that have been recognized as least ordered (Acharya *et al.*, 1990), such as residues 12, 251 to 256, 315, 554 and 836 to 840. Residues Asp339 and Val436 are on surface loops, and residues Asn678 and Glu730 occur at the start of α helices. All these residues are in reasonable electron density but probably contain positional errors. Residues Tyr203 and Ser210 were carefully examined in the native GP*b*, and their unusual conformations are supported by density and structural features (Acharya *et al.*, 1990). Ser210 is on a surface loop and this loop has poor electron density in the R state structures but satisfactory density in the T state structure.

(c) *Structure analysis*

Protein co-ordinates and electron density maps were examined on an Evans and Sutherland PS300 on-line to a VAX 6210 computer with the program FRODO (Jones, 1978), modified by J. W. Pflugrath, M. Saper, R. E. Hubbard and P. R. Evans. Superimposition of protein structures were performed by the program SUPERSIEVE (D.B., unpublished results) adapted from

the least-squares superimposition algorithm of S. J. Remington based on the method of Kabsch (1978). The program provides the facility of defining a sub-set of atoms that superimpose within a desired r.m.s. deviation. The method involves determination of an initial matrix for the superimposition of 2 structures and calculation of the overall r.m.s. difference. When this difference is larger than the desired value, the atom pair that deviate most between the 2 structures is removed from the set of co-ordinates and a superimposition is performed on the selected sub-set. This process is continued until the sub-set of atoms is obtained that superimpose to within the desired r.m.s. difference. In this work, a core of atoms whose C^{α} positions superimpose to within an r.m.s. difference of 0·5 Å was defined. Application of the matrix determined for these core atoms to the whole molecule resulted in a larger number of atoms that superimpose more closely than occurred after a global least-squares superimposition.

Solvent accessibility calculations were performed using the algorithm of Lee & Richards (1971), as implemented by T. J. Richmond with a water probe radius of 1·4 Å.

3. Results

(a) *R state GP*a

(i) *Global conformation*

Tetrameric R state GP*a* displays 222 symmetry of approximately equivalent subunits with C^{α} positions of all subunits deviating from the mean by an r.m.s. distance of 0·31 Å, a value that is similar to that observed for the four subunits of R state GP*b*. At the catalytic site of all four subunits of GP*a*, Arg569 interacts with a sulphate ion of crystallization bound at the substrate phosphate recognition site. In R state GP*b*, Arg569 contacts the sulphate group in only two of the subunits (Barford & Johnson, 1989). Thus, the Ser-P-activated enzyme exhibits a more homogeneous constellation of atoms at the catalytic site than the sulphate-activated GP*b*.

The quaternary and tertiary structures of R state GP*a* are essentially identical to those of R state GP*b*, except for small differences in the vicinity of the Ser-P site and the small difference between subunits noted above. The proteins crystallize with identical space groups and unit cell dimensions. After superimposing equivalent pairs of R state GP*a* and GP*b* subunits, the average r.m.s. deviation between C^{α} atoms is 0·67 Å (Table 2). Between each pair, on average, 15 C^{α} atoms differ by more than 2·0 Å. On excluding these atoms, the average r.m.s. deviation between subunit pairs is 0·55 Å. This compares to an average r.m.s. deviation of 0·58 Å between all corresponding pairs of subunits of a GP*a* tetramer or 0·57 Å if C^{α} atoms for each subunit pair (average of 2/subunit) differing by more than 2·0 Å are excluded. The largest differences between R state GP*a* and GP*b* occur in parts of the structure that are poorly located in the electron density, are thus undefined and subject to differences in interpretation. In addition, these regions of the structure differ most and, to a similar extent, between equivalent subunits within GP*a* or GP*b* tetramers, suggesting conformational variability and disorder within these regions. Within the data precision, the tertiary conformations represented by C^{α} positions of R state GP*a* and GP*b* are identical. The mean r.m.s. deviation between C^{α} atoms of the two pairs of equivalent dimers is 0·68 Å (or 0·57 Å on excluding 32 C^{α} atoms from each pair of dimer that differ by more than 2 Å). Thus, the quaternary structures of the dimers are also identical to within the precision of the data. GP*a* and GP*b* tetramers also superimpose to within similar values (Table 2).

The only significant but small difference in side-chain positions between R state GP*a* and GP*b* (apart from that noted above at the catalytic site) occurs at the Ser-P site and results from the fact that in GP*b* the Ser-P group is mimicked by a non-covalent association of Ser14 with a sulphate of

Table 2

Superimposition of refined co-ordinates

A. *R state GP*b *onto R state GP*a

Structure	r.m.s. deviation	Atoms deviating > (Å)	No. of atoms excluded
Av. monomer	0·667	0·0	—
	0·551	2·0	15
Av. dimer	0·676	0·0	—
	0·566	2·0	32
Tetramer	0·675	0·0	—
	0·558	2·0	61
Superimposition of all possible pairs of GP*a*, average values given			
	0·583	0·0	—
	0·566	2·0	2

B. *R state GP*b *onto R state GP*b*–AMP complex*
*R state GP*a *onto R state GP*b*–AMP complex*

	GP*b*	GP*a*	GP*b*	GP*a*	GP*b*	GP*a*
Av. monomer	0·586	0·592	0·0		—	—
	0·562	0·533	2·0		4	7
Av. dimer	0·618	0·603	0·0		—	—
	0·598	0·545	2·0		7	13
Tetramer	0·630	0·616	0·0		—	—
	0·614	0·557	2·0		11	30

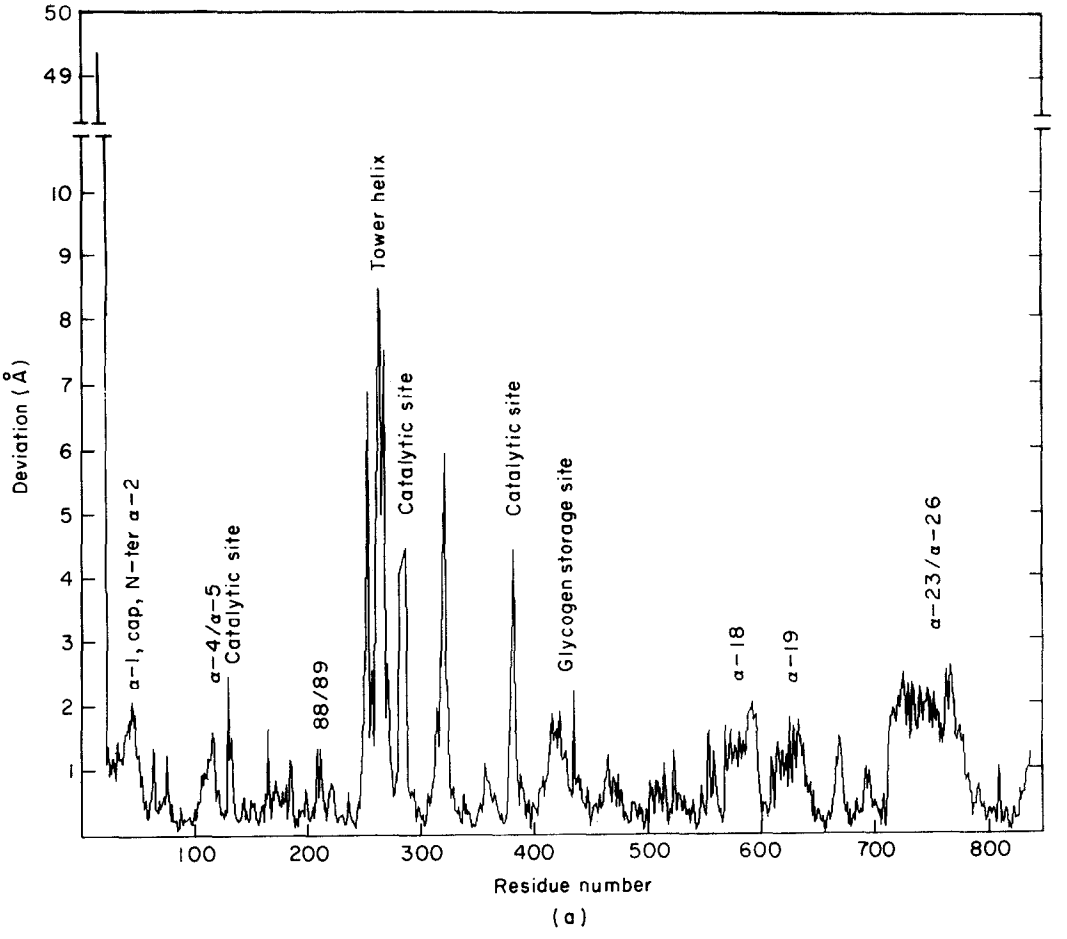
Deviation (Å)
Residue number
α-1, cap, N-ter α-2
α-4/α-5
Catalytic site
88/89
Tower helix
Catalytic site
Catalytic site
Glycogen storage site
α-18
α-19
α-23/α-26

(a)

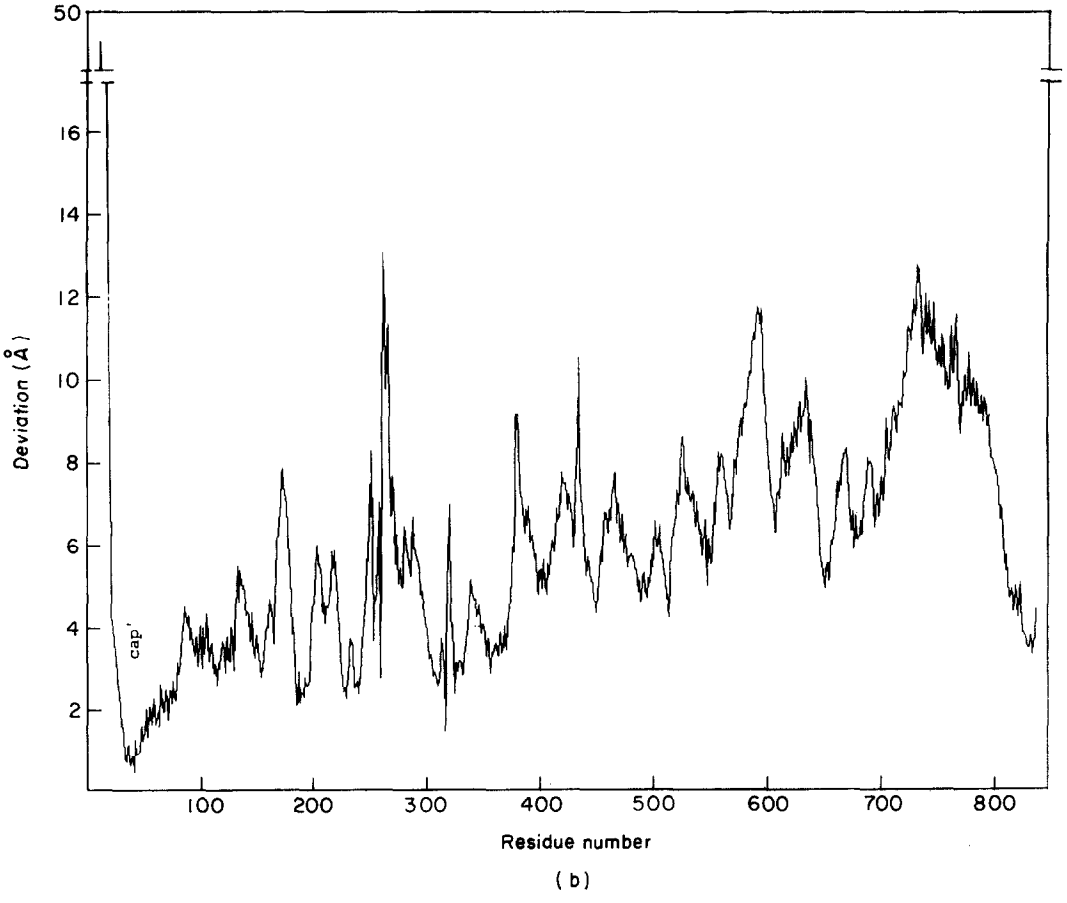
Deviation (Å)
Residue number
cap'

(b)

crystallization. The serine residue of GP*a* is displaced by 0·75 Å relative to that of GP*b* and the position of the phosphate group of the Ser-P is displaced by 1·0 Å relative to the sulphate group in GP*b*, reflecting the differences between the covalent and non-covalent association of the dianion (Fig. 2). The guanidinium side-chains of Arg43′ and Arg69 of GP*a* are displaced by 1·0 Å relative to GP*b* in order to optimize interactions to Ser-P rather than sulphate.

On transition from T state GP*b* to R state GP*a*, a significant conformational change occurs that is similar to the conformational change noted between T state GP*b* and R state GP*b* (Barford & Johnson, 1989). After a least-squares superimposition of one subunit (subunit 1) of T state GP*b* onto one subunit (subunit 1) of R state GP*a*, the overall r.m.s. deviation of C^{α} co-ordinates is 3·6 Å or 1·3 Å if residues 10 to 21 are excluded. A conserved core representing 66% of the C^{α} atoms superimpose within an r.m.s. deviation of 0·5 Å, and there is no indication of shifts of one domain relative to another. Thus, a significant proportion of the subunit undergoes no tertiary structural change. Those regions of the structure outside the core that deviate significantly between the two structures are associated with (1) the subunit–subunit interface (the N-terminal residues 10 to 24; the α1 helix residues 23 to 38; the cap residues 39 to 46; the N-terminal region of the α2 helix residues 46 to 49; the α4 helix residues 112 to 118; the tower helix 280s loop residues 260 to 286 and the C-terminal residues 838 to 842); (2) residues that contribute to the catalytic site; (3) the dimer–dimer interface (α12 of the glycogen storage site and helices α18, α19 and α23 to α26); and (4) the disordered flexible regions (residues 252 to 256 and 313 to 324). These differences are shown in Figure 5(a), where the matrix was obtained from superimposition of the core residues. A measure of the quaternary conformational change of functional dimers of glycogen phosphorylase can be obtained by transforming both subunits of the T state GP*b* dimer onto the R state GP*a* dimer where the matrix is derived from least-squares superposition of the core residues of subunit 1. The C^{α} atoms of dimers deviate by 7·3 Å (or 6 Å if residues 10 to 21 are excluded) and the magnitude of the differences in individual residues is shown in Figure 5(b). The quaternary conformational change can be described as a rotation of one subunit relative to the other by 10° about an axis approximately perpendicular to the molecular 2-fold axis, positioned close to the cap′/α2 interface. This draws the subunits together at the cap′/α2 interface and apart at the tower–tower interface (Fig. 1(e) and (f)). The quaternary conformational change is promoted through the concerted but localized conformational change at the cap′/α2 interface represented by the N-terminal residues, the helices α1′, α2′, α4′ and cap′ of one subunit and α2 helix of the opposite subunit. The quaternary conformational change affects the relative disposition of the tower helices, transmitting a signal to the catalytic site (Barford & Johnson, 1989). The structural changes on activation also promote dimer association to tetramers. The changes at the dimer–dimer interface will be described in detail elsewhere. Here, the nature of the conformational changes at the cap′/α2 interface associated with phosphorylation and the communication of these changes to the allosteric site are described.

(ii) *Conformational changes at the cap′/α2 interface*

The structural changes between T state GP*b* and R state GP*a* occur in the vicinity of the cap′/α2 interface to form a surface complementary to the phosphorylated N-terminal residues (10 to 18). The major change involves the ordering and repositioning of the N-terminal tail and the displacement and disorder of the C-terminal residues 838 to 842. A concerted tertiary conformational change (of about 1·2 to 2 Å in C^{α} positions) takes place for the self-contained structural unit formed by the α1 helix, cap, N terminus of α2, α4 helix, and the loop connecting α4 with α5. The unit rotates 4° almost as a rigid body, so that superimposition of equivalent residues of this unit between R state GP*a* and T state GP*b* results in an r.m.s. deviation of only 0·5 Å. If the tertiary structure changes were to occur without the corresponding quaternary change, they would result in a movement of the cap′ relative to the α2 helix of the other subunit. The tertiary changes are apparent in Figure 6, where subunit 1 is coloured turquoise (T state) and orange (R state). The tertiary changes shift the cap (turquoise to orange) in a direction towards the N terminus of helix α2′ in subunit 2 (T state, purple). The quaternary change partially counteracts this movement and shifts α2′ (T state, purple, to R state, yellow). These compensatory conformational changes are apparent at the other interface (right-hand side in Fig. 6), where the combined tertiary and quaternary changes result in little overall change in the disposition of the cap′ relative to the α2 helix. The compensatory shifts are apparent also in Figure 5. In Figure 5(a) there are significant tertiary changes in residues 35 to 45 of subunit 1 (between 1·2 and 2·1 Å) but in Figure 5(b) the quaternary change results in less displacement (between 0·5 and 1·3 Å) of these residues in subunit 2 (corresponding to residues with a prime in Fig. 6), in comparison to the generally greater displacement of residues in subunit 2 resulting from the quaternary change. The compensatory tertiary and

Figure 5. The r.m.s. deviation in C^{α} atoms between R state GP*a* and T state GP*b* after superposition of core atoms in subunit 1 that differ by less than 0·5 Å. (a) Subunit 1 GP*a* onto subunit 1 GP*b* showing tertiary structure changes. (b) Subunit 2 GP*a* onto subunit 2 GP*b* showing changes resulting from both tertiary and quaternary conformational changes. Some key structural elements are marked. For further details, see the text.

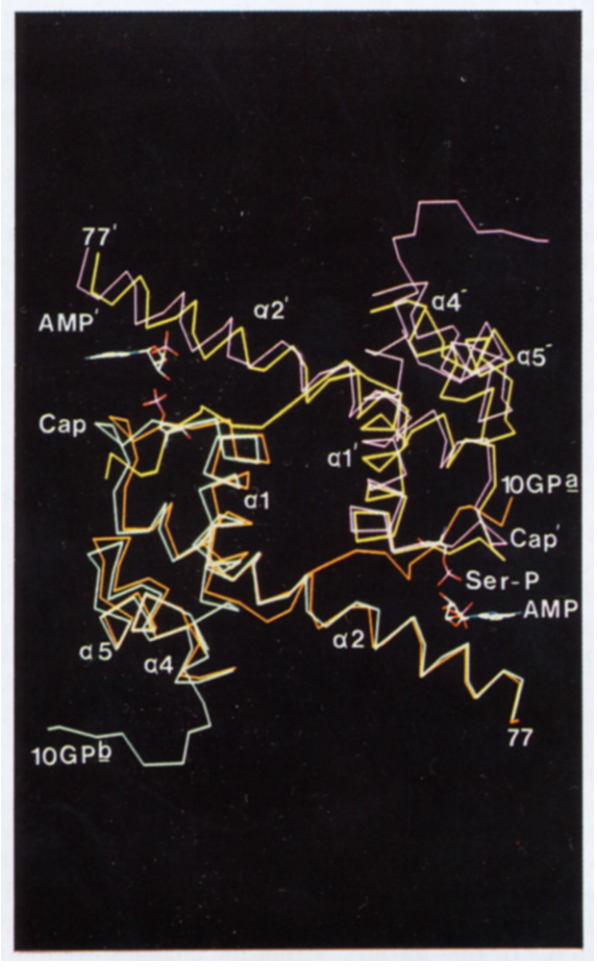

Figure 6. A colour diagram illustrating tertiary and quaternary structural changes at the cap′/α2 helix interface. The view is down the 2-fold symmetry axis of the dimer similar to Fig. 1(a) and (b). Subunits 1 and 2 of T state GP*b* are shown turquoise and purple, respectively, and for R state GP*a* orange and yellow, respectively. Subunits 1 of the T and R states have been superimposed on the basis of the core residues. Tertiary structural changes in subunit 1 in the vicinity of the cap are apparent from the changes between turquoise and orange structures at the left-hand side of the Figure. The combined tertiary and quaternary changes are apparent from the changes in positions of subunits 2 (purple and yellow structures). The quaternary structural changes result in greater changes between subunits 2 of the T and R states, with the exception of the cap residues, where the quaternary changes partially compensate the tertiary changes (right-hand side of the Figure).

quaternary changes allow the cap′ to interact more closely with the symmetry-related α2 helix in the vicinity of residues 42′ to 45′, and enable both the cap′ and α4′ helix to maximize interactions with Ser-P and the re-structured N-terminal tail. The compensatory shifts allow residues 39′ to 41′ of the cap′ to conserve interactions with the β7 strand (a salt-bridge between Lys41′ and Glu195, and H bonds between main-chain carbonyl groups of Leu39′ and Val40′ with Arg193) as shown in Figure 7. The β7 strand, which is part of the conserved core, does not undergo tertiary conformational change.

A localized conformational change within the α2 helix facilitates these structural changes (Fig. 8). In T state GP*b*, the α2 helix is unwound between His62 and Gly65, with a turn of 3_{10} helix between Asp61 and Val64 (Fig. 8(b)). This marks a structural discontinuity in the helix and a point where the helix bends by 30°. Unwinding extends the helix along its axis. In T state GP*b*, the side-chain of His36′ intercalates between the side-chains of Val64 and Ile68, and forms a salt-bridge to Asp838 of the C terminus. Phe37′ packs between Asp61 and Leu64 of the α2 helix and against His36′ of the cap′. The presence of Phe37′ in this position appears to make a significant contribution to the unwinding force on the helix through a packing interaction with Leu64. Model-building studies show that a more regular helix would cause steric conflict between these two residues. On transition to GP*a*, disordering of the C-terminal residues 838 to 842 and motion of the cap′ ruptures the His36′–Asp838 salt-bridge. Subsequent rotation of His36′ by 120° about its C^{α}–C^{β} bond into a previously unoccupied cavity and a 70° rotation of Phe37′ about its C^{β}–C^{γ} bond remove the unwinding force on the α2 helix, allowing it to contract by shifting residues 48 to 64 from the N terminus by about 0·75 Å (turquoise to orange in Fig. 6; Fig. 8(a)). The contraction of the α2 helix arising from shifts of the N-terminal residues is correlated with shifts in the cap and α1 helix, which in turn interact with the α2′ helix of the other subunit. Linked conformational changes result in a concerted response in both subunits with conservation of symmetry. In R state GP*a*, a salt-bridge is formed between the side-chains of Arg33′ of α1′ and Asp61 of α2. This interaction is assisted by the motion of the α1′ helix and side-chain rotation of Arg33′ (Fig. 8). In addition, the new position of His36′ facilitates and stabilizes the transition to the R state by preventing steric conflict with Ile68 as the cap′ moves towards the α2 helix following the conformational changes. The overall motion of the cap′ relative to the α2 helix produced by the quaternary and tertiary conformational change is approximately 0·8 Å (Fig. 5(b)).

(iii) *Interactions by the phosphorylated N-terminal tail*

The interactions made by the phosphorylated N-terminal tail that promotes these changes involve

Figure 7. The cap′/β7 subunit–subunit interactions. The view is approximately normal to the 2-fold axis of the dimer and the 2-fold axis is vertical. (a) R state GP*a*; (b) T state GP*b*; and (c) R state GP*a* (thick lines) and T state GP*b* (thin lines) compared. The cap of subunit 1 (no superscript) is shown at the left and that of subunit 2 (prime) is shown at the right. There is no tertiary structural change in β7 (subunit 1). The compensatory tertiary and quaternary structural changes are apparent in the closer superposition of the cap′ residues in subunit 2 compared to those of subunit 1. The shifts conserve the interactions between the cap′ and β7 for both subunits.

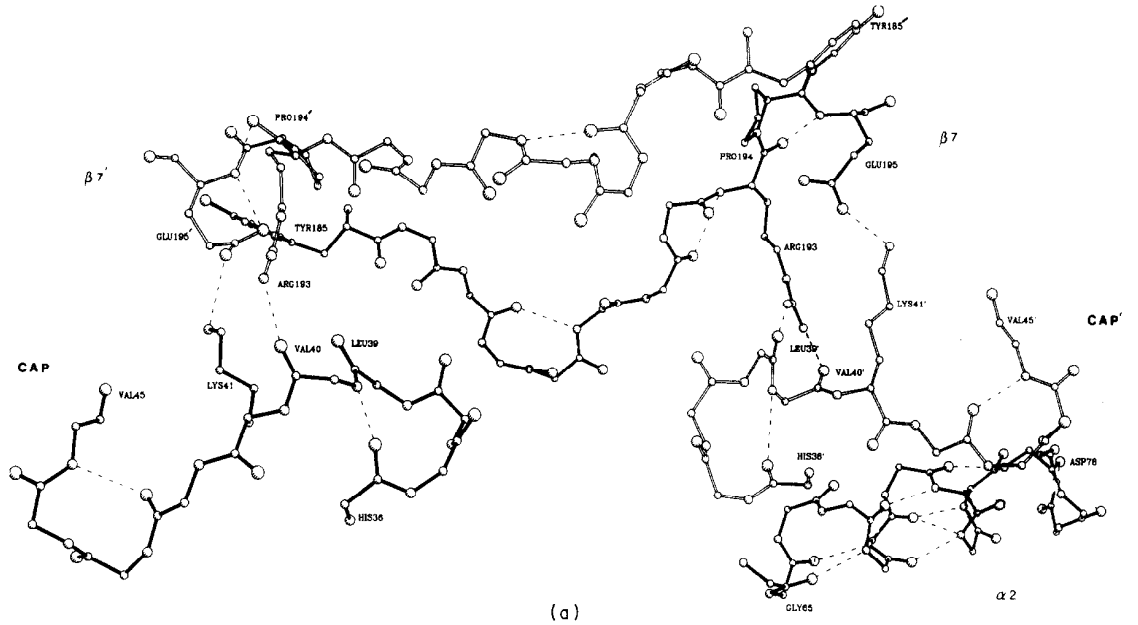
TYR185'
PRO194'
β7'
PRO194
β7
GLU195
GLU195'
TYR185
ARG193
ARG193'
LYS41'
VAL45'
CAP'
CAP
LEU39'
VAL40
LEU39
VAL40'
LYS41
VAL45
HIS36'
ASP78
HIS36
GLY65
α2

(a)

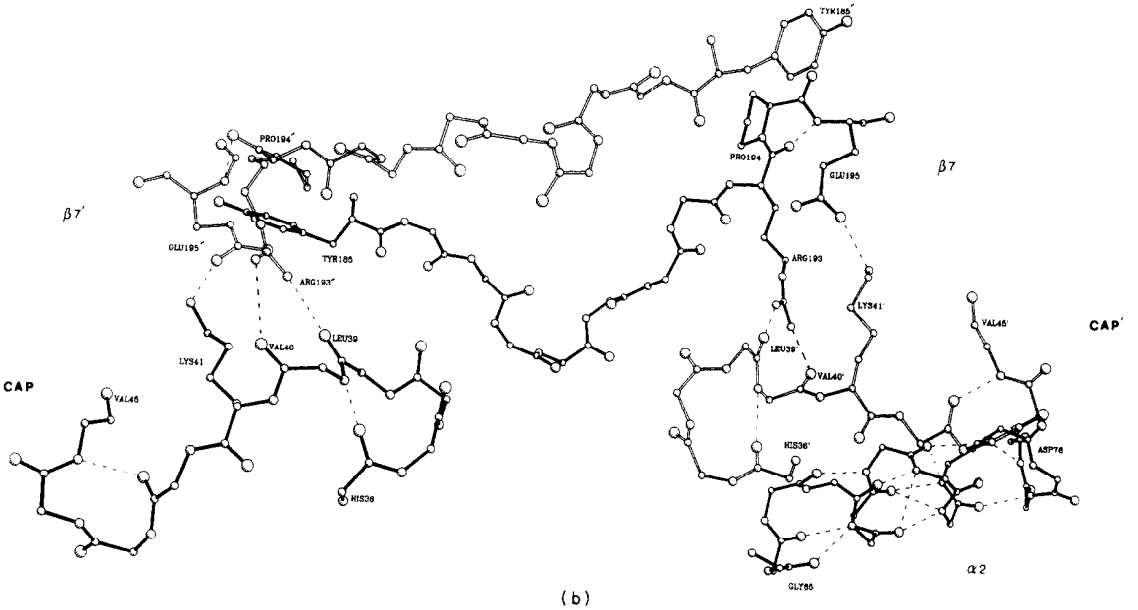
TYR185'
PRO194'
PRO194
β7'
β7
GLU195'
GLU195
TYR185
ARG193'
ARG193
LYS41
VAL45'
CAP'
CAP
LEU39'
LEU39
VAL40'
VAL40
LYS41'
VAL45
HIS36'
ASP78
HIS36
GLY65
α2

(b)

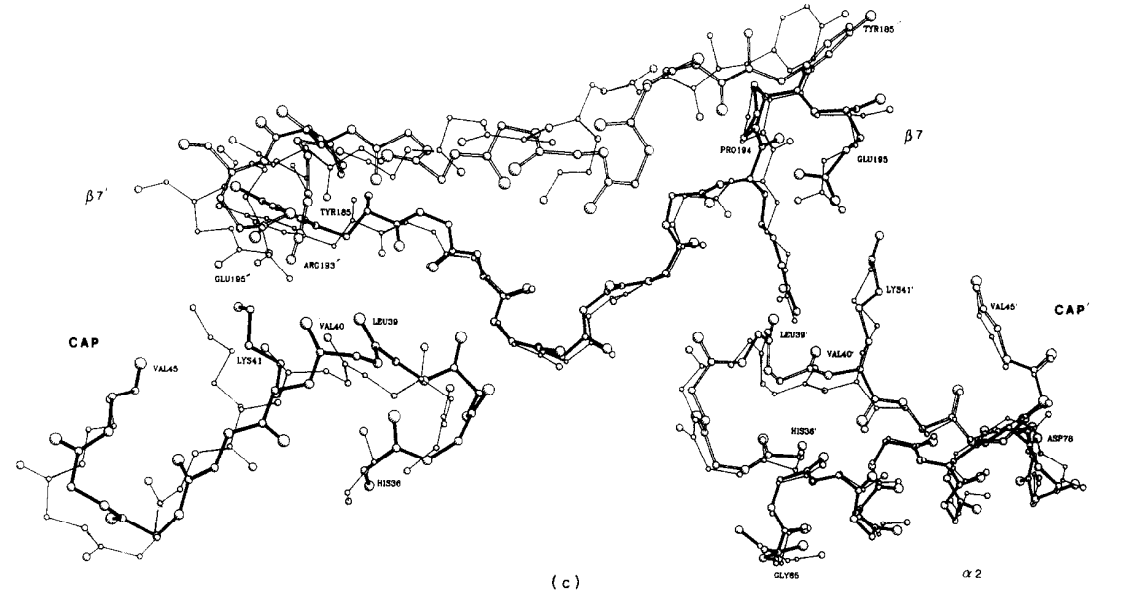
TYR185'
PRO194
β7
β7'
GLU195
TYR185
ARG193'
GLU195'
LYS41'
VAL45'
CAP'
CAP
LEU39'
VAL40
LEU39
VAL40'
LYS41
VAL45
HIS36'
ASP78
HIS36
GLY65
α2

(c)

Fig. 7.

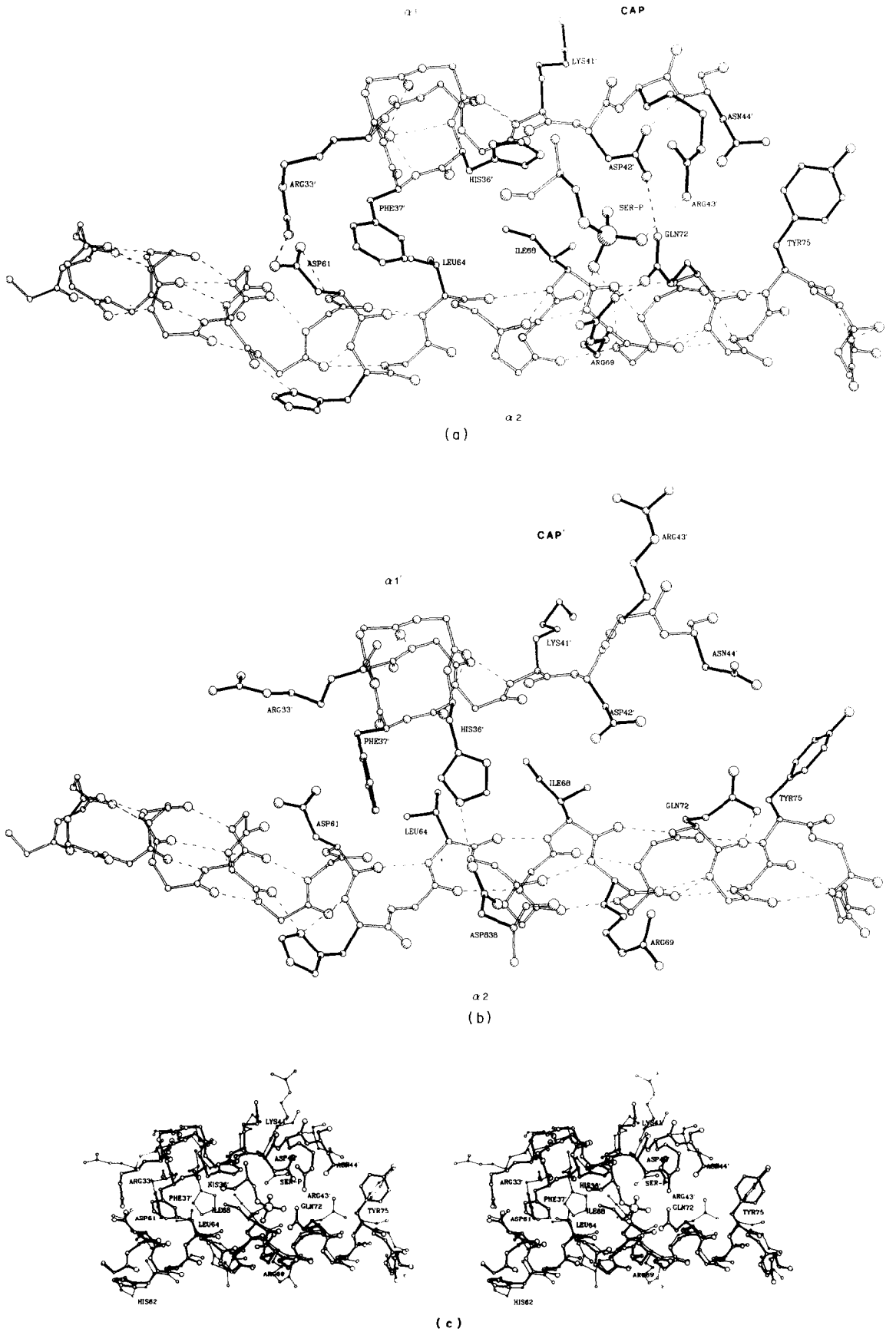

Figure 8. The cap'/α2 helix interactions. Subunit 1, no superscript; subunit 2, superscript. The view is down the 2-fold axis of the dimer but rotated 180° about this axis with reference to Fig. 5, so that the interactions in this view represent those at the top left of Fig. 5. (a) R state GP*a*; (b) T state GP*b*; and (c) a stereo diagram of R state GP*a* (thick lines) and T state GP*b* (thin lines) compared. For further details, see the text.

Table 3
*Dihedral angles for N-terminal residues in T state GP*b *and R state GP*a

Residue	T GP*b* ϕ (deg.)	T GP*b* ψ (deg.)	T GP*b* Conformation	R GP*a* ϕ (deg.)	R GP*a* ψ (deg.)	R GP*a* Conformation
Lys11			Poorly defined	−70	−17	α
Gln12			Poorly defined	−80	−4	α
Ile13	−175	60	β	−90	100	β
Ser14	−78	170	β	−154	136	β
Val15	−81	81	β	−70	−19	α
Arg16	−113	29	β	−44	−40	α
Gly17	125	173		−80	−31	α
Leu18	−124	97	β	−89	115	β
Ala19	−75	83	β	112	132	Left-handed
Gly20	−97	132	β	−119	115	β
Val21	−42	−53	α	74	−32	Left-handed
Glu22	−59	−58	α	83	34	Left-handed
Asn23	−45	−44	α	−89	134	β
Val24	−64	−33	α	−56	−31	α
Thr25	−68	7	α	−54	−72	α

residues from both subunits of the interface. On phosphorylation of Ser14, the N-terminal tail (residues 10 to 18) changes conformation from a mostly β structure, which makes intra-subunit contacts, to a partially coiled structure that makes inter-subunit contacts.

In T state GP*b*, residues 10 to 18 are poorly ordered and adopt an irregular extended conformation (Table 3; Fig. 6). Interactions are made with helices α3, α4 and α16. The Ser14 side-chain is shielded by Glu501 and there are hydrogen bonds between Arg16 and Glu105, Gln96 and Val493 (main-chain O: Martin *et al.*, 1990; Acharya *et al.*, 1990). Helix α1 begins at residue 20. Phosphorylation of Ser14 results in a radical restructuring of the N-terminal residues. The first half-turn of the α1 helix becomes unwound at Asn23 and residues 10 to 22 are orientated approximately 120° in the opposite direction to that of T state GP*b* (Fig. 6). Arg10 shifts 50 Å on the transition from T state GP*b* to R state GP*a*. There is a turn of 3_{10} helix between Arg10 and Ile13, and between Val15 and Leu18. In addition, the O^{γ} atom of Ser14 makes a hydrogen bond to the N of Arg16 and this turn is reinforced by a hydrogen bond from a phosphate oxygen atom to Arg16 (Fig. 9). Residues 10 to 18 have the appearance of a distorted helix, although residues 13 and 14 have a β conformation (Table 3). Residues 18 to 22 have an irregular conformation, with some left-handed residues. Thus, the non-phosphorylated and the phosphorylated N-terminal peptides have quite different conformations. In both GP*b* and GP*a*, residues 1 to 9 are not visible in the electron density map.

Table 4
Interactions made by N-terminal tail

A. *Salt-bridges and H bonds <3·5 Å*	
Arg10 NH2	Gly116′ O
Lys11 O	Arg43′ NH2
Gln12 OE1	Lys28′ NZ
Ile13 O	Arg43′ NH2
Ser14-P O-2	Arg43′ NH1, Arg43′ NH2
Ser14-P O-3	Arg69 NH1, Arg69 NH2
Ser14-P O-4	Arg69 NH1
Ser14-P N	Asn32′ OD1
Ser14-P O	His36′ NE2
B. *van der Waals' contacts <4·0 Å*	
Arg10	Arg43′ (cap), Leu115, Gly116′, Leu117′
Lys11	Arg43′ (cap)
Gln12	Lys28′, Asn32′, Leu115′
Ile13	Phe31′, Asn32′, Arg43′, Tyr51′, Leu115′, Leu117′
Ser14-P	Asn32′, His36′
Val15	His36′, Ile68, Arg69
Arg16	Arg69
Leu18	Phe37′

The N-terminal tail of R state GP*a* interacts with the α2 helix and the cap′ and C-terminal region of helix α4′ from the other subunit. Details are summarized in Table 4. The Ser-P site is created from the guanidinium side-chains of Arg43′ of the cap′ and Arg69 of the α2 helix, which form salt-bridges to the dianionic phosphate group. These interactions are made possible by the change in position of α2 relative to the cap′ and side-chain rotations of Arg43′ and Arg69 (Fig. 9). The side-chain of Ile13 inserts into a hydrophobic pocket formed from the side-chains of Phe31′, Arg43′, Tyr51′ and Leu117′ with a hydrogen bond formed between the main-chain carbonyl group of Ile13 and side-chain of Arg43′. Motion of His36′ on conversion to GP*a* removes a possible steric conflict with Ile13. Similarly, the Val15 side-chain packs into a hydrophobic pocket formed by the side-chains of Ile68, Arg69 and His36′. Leu18 packs against Phe37′ of the cap′. Arg10 occupies the site previously taken by Arg43′ of T state GP*b* with the main-chain N and side-chain forming hydrogen bonds with the main-chain carbonyl groups of Leu115′ and Gly116′, respectively. Again, the correct position of Leu115′ and Gly116′ relative to the N-terminal tail is achieved through quaternary and tertiary conformational changes. The conformation of the phosphorylated N-terminal tail causes a disordering of

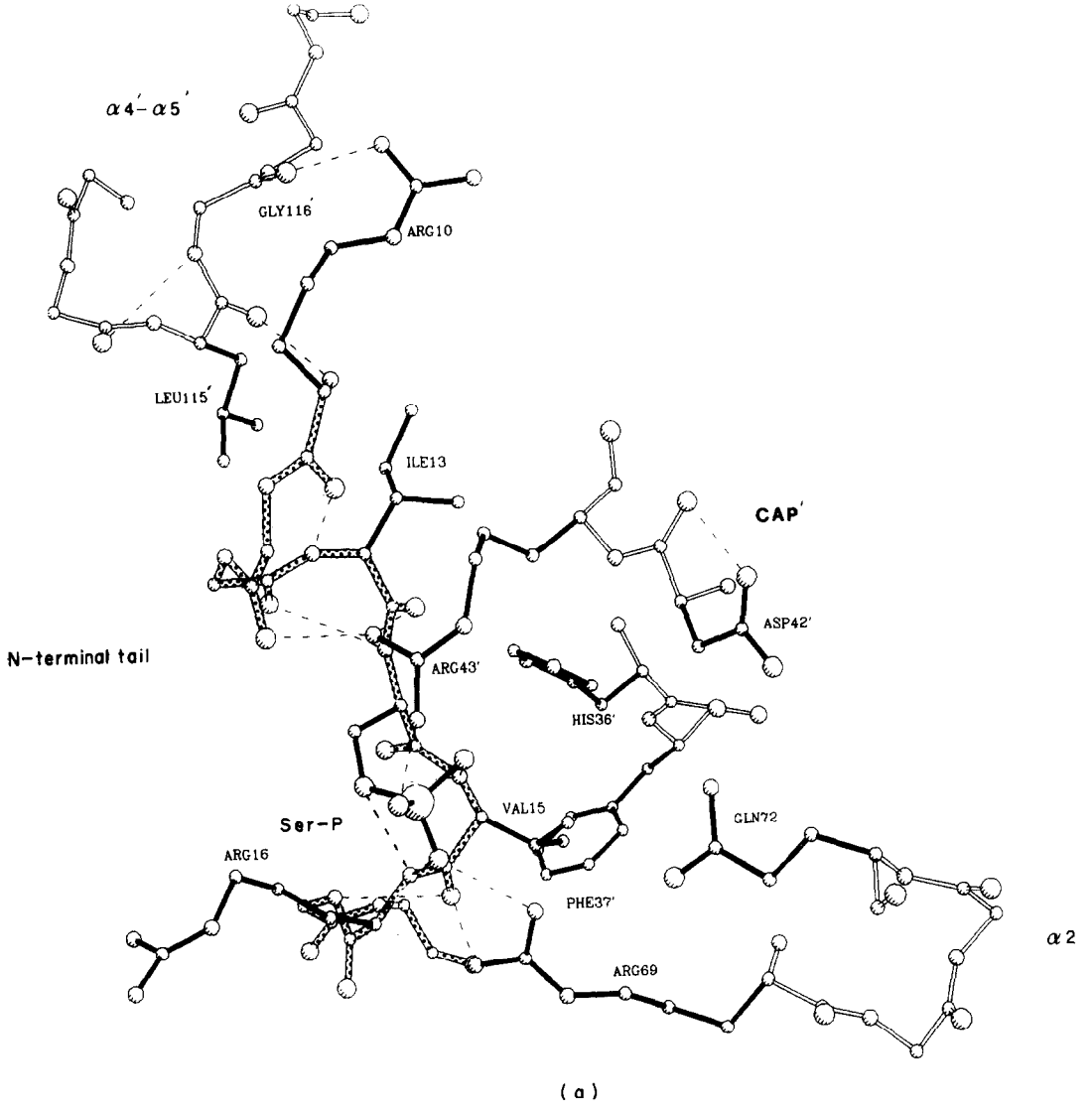

Figure 9. The cap′/N-terminal tail and C-terminal tail interactions. (a) R state GP*a*. Main-chain residues 10 to 16 for GP*a* are shown dotted. (b) T state GP*b*. (c) A stereo diagram of R state GP*a* (thick lines) and T state GP*b* (thin lines) compared.

C-terminal residues 838 to 841. The site previously occupied by residues 838 to 841 of T state GP*b* is occupied by residue Arg16. Disordering of the C terminus ruptures a salt-bridge between Asp838 and His36′ of the cap′, as described above. As noted by Martin *et al.* (1990), the conformational change results in a change in environment of Ser14 from one that contains clusters of negatively charged groups in the non-phosphorylated state to one that contains clusters of positively charged groups in the phosphorylated state. In T state GP*b*, there are 11 acidic and seven basic residues within 15 Å of the C^{α} atom of Ser14 (excluding residues 10 to 20). In R state GP*a*, there are six acidic and 11 basic residues.

The conformational changes on the T to R transition that create the Ser-P recognition site also lead to interactions that are important in developing a high-affinity AMP effector site situated 15 Å from the Ser-P site. In the R state, side-chain rotations allow a hydrogen bond between Asp42′ of the cap′ and Gln72 of α2 and between Arg69 and Gln72 (Fig. 9).

(b) *AMP complexes*

(i) *T state AMP complex*

The global conformation of the refined T state GP*b*–AMP subunit structure is closely similar to native T state GP*b* co-crystallized in the presence of 2 mM-IMP (r.m.s. deviation in C^{α} positions is 0·3 Å). The major conformational differences between T state GP*b* and the AMP complex are associated with the more flexible regions of the molecule (residues 251 to 258 and 319 to 323), where C^{α} atom positions differ by 1·0 to 2·5 Å.

The AMP allosteric site is composed of a cleft at the interface of the two subunits. The floor of the cleft is formed by the juxtaposition of the C termini

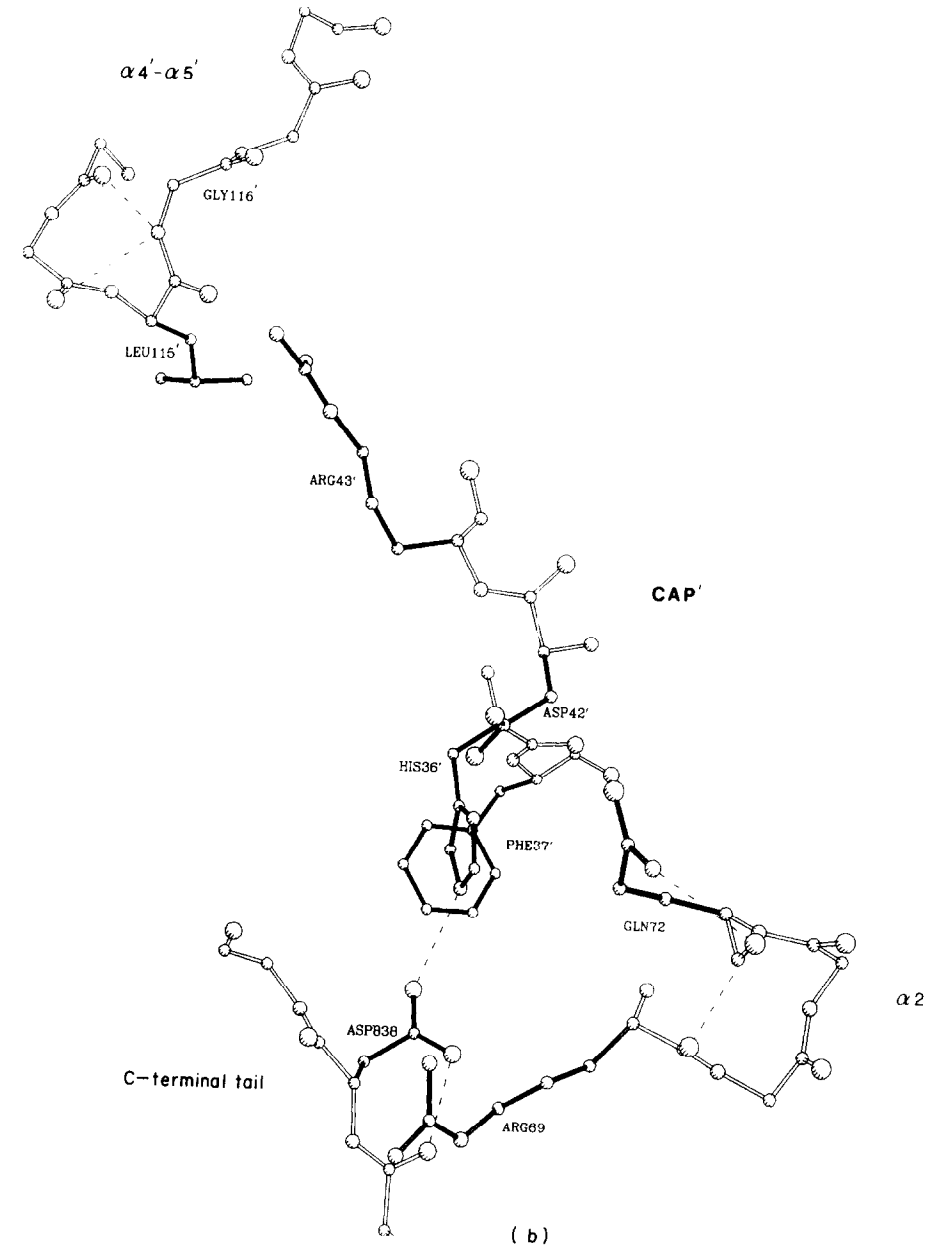
α4'-α5'
GLY116'
LEU115'
ARG43'
CAP'
ASP42'
HIS36'
PHE37'
GLN72
α2
ASP838
C-terminal tail
ARG69
(b)

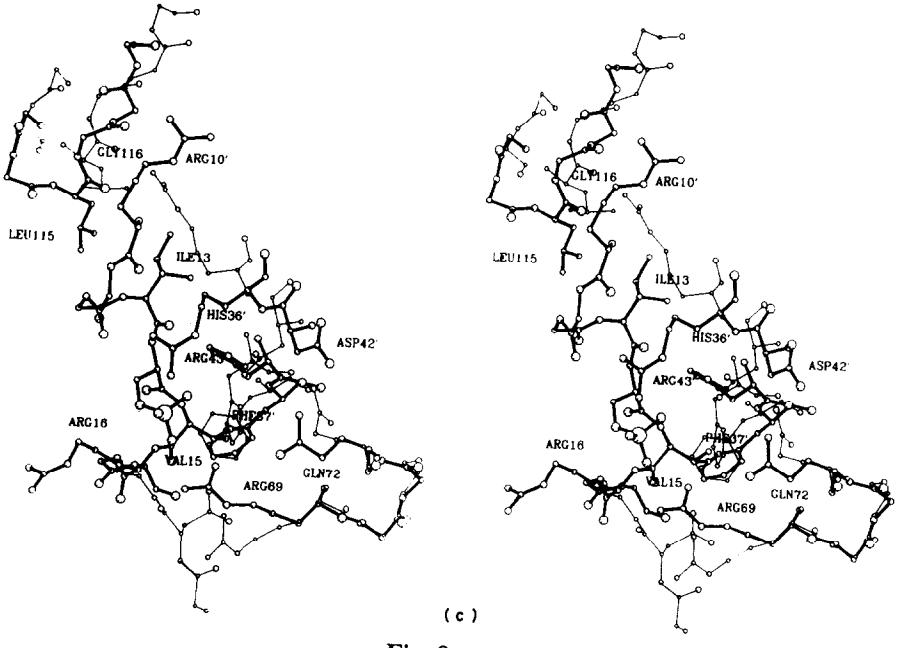
GLY116
ARG10'
LEU115
ILE13
HIS36'
ASP42'
ARG43'
ARG16
PHE37'
GLN72
ARG69
(c)

Fig. 9.

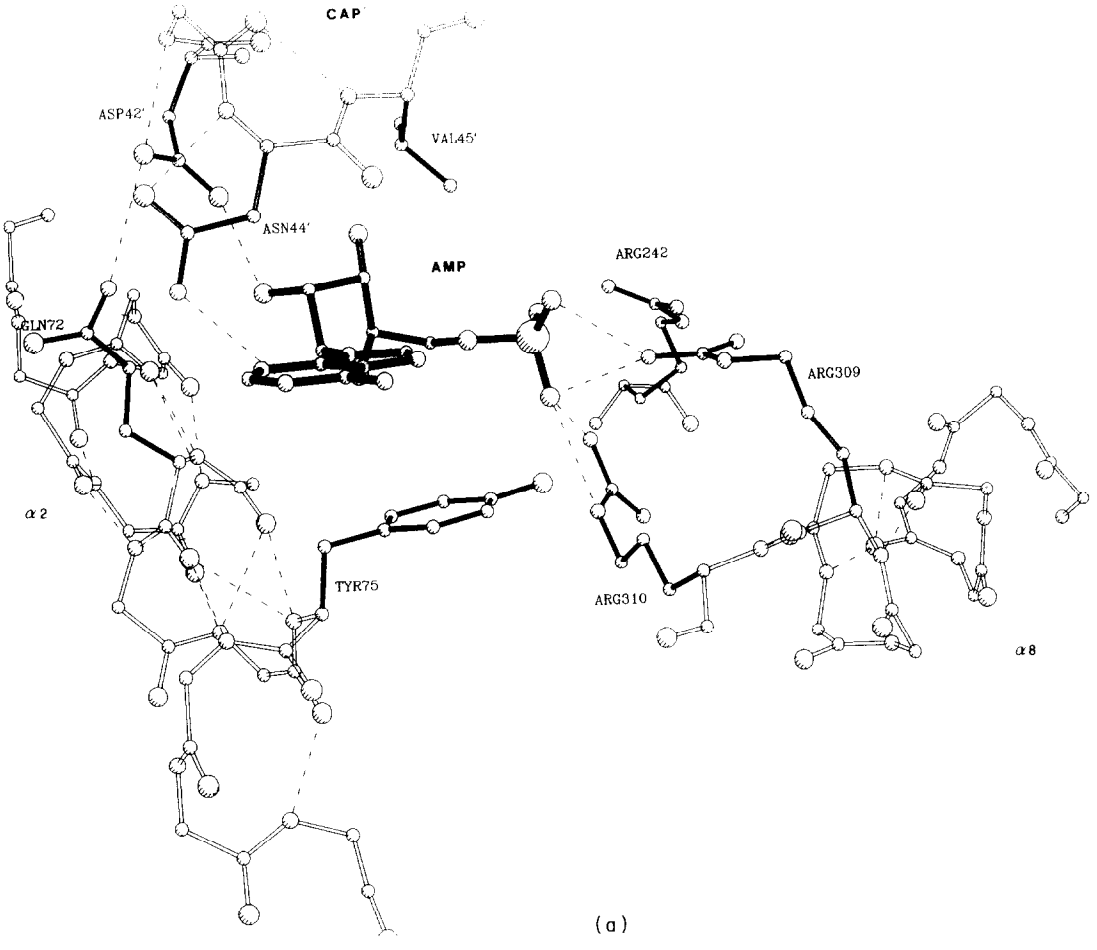
CAP
ASP42'
VAL45'
ASN44'
AMP
ARG242
GLN72
ARG309
α2
TYR75
ARG310
α8

(a)

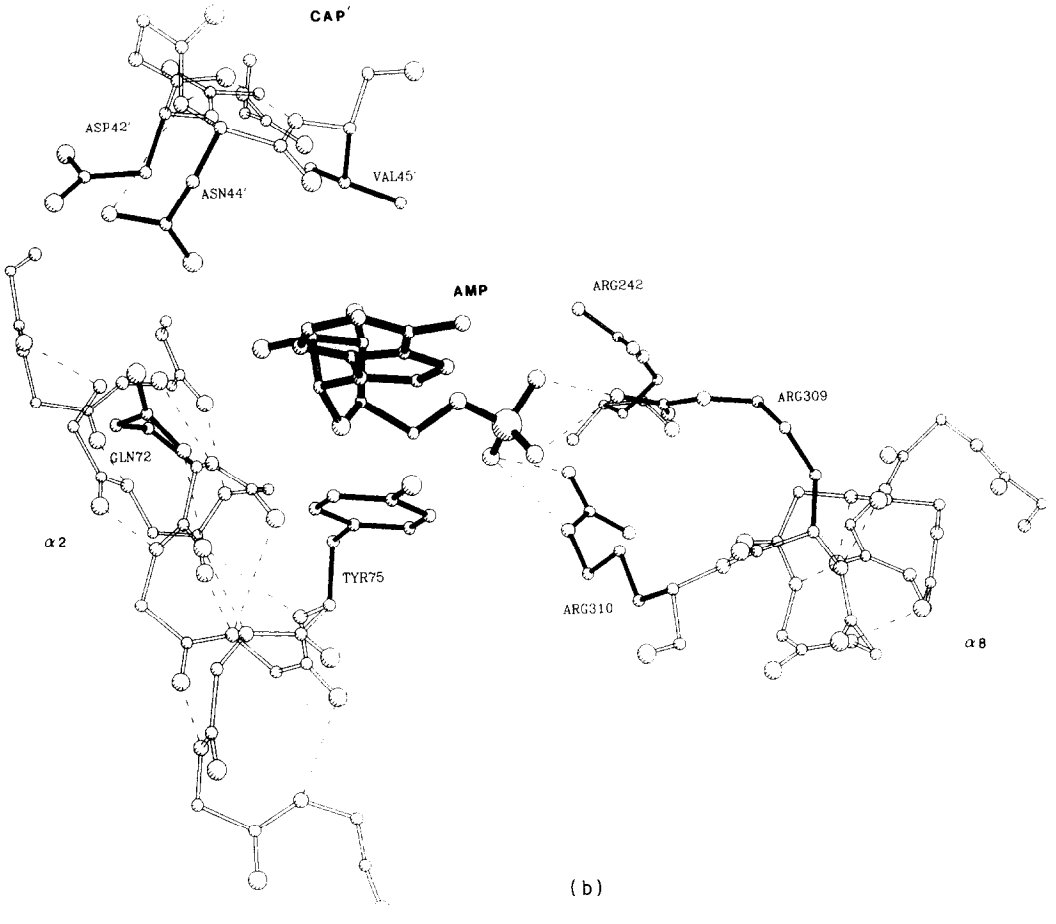
CAP'
ASP42'
VAL45'
ASN44'
AMP
ARG242
ARG309
GLN72
α2
TYR75
ARG310
α8

(b)

Fig. 10.

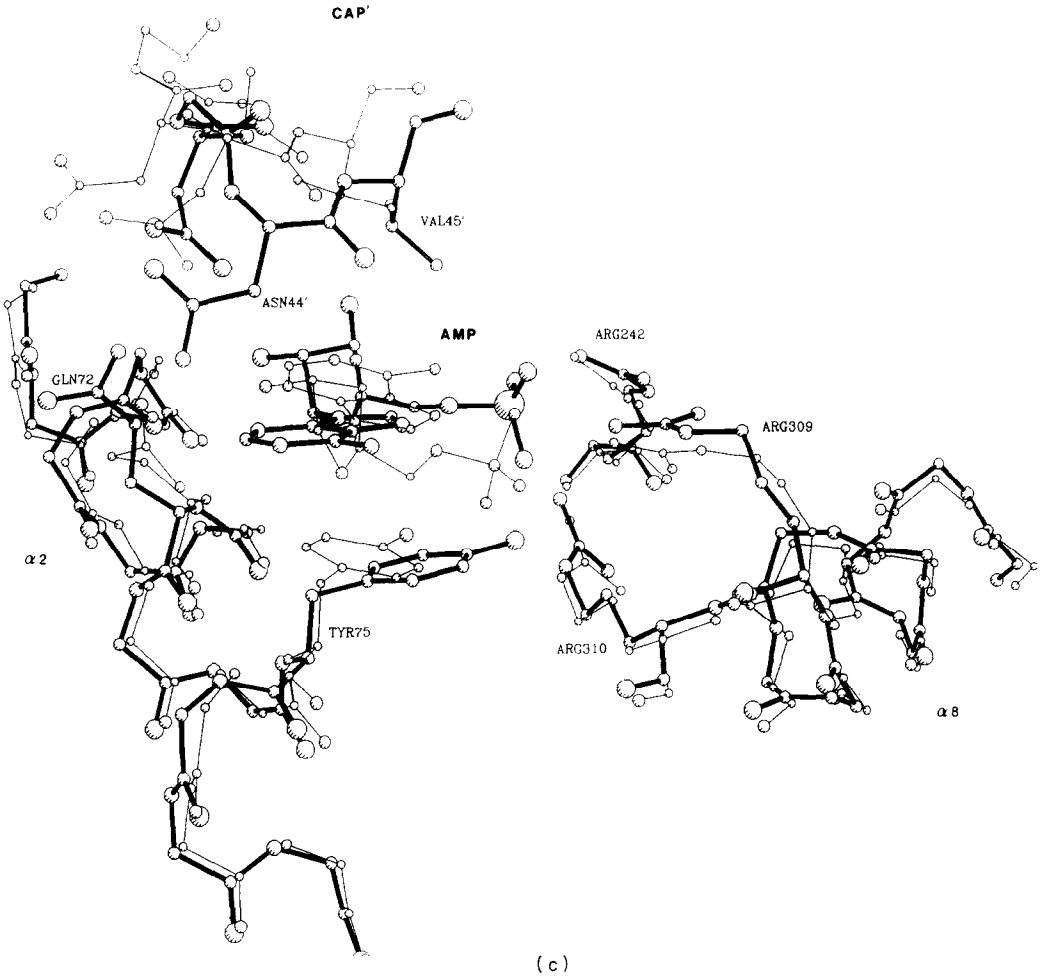

Figure 10. AMP interactions. The view is down the axis of the α2 helix. (a) R state GP*b*; (b) T state GP*b*; and (c) R state GP*b* (thick lines) and T state GP*b* (thin lines) compared.

of the α2 and α8 helices, forming a V. A portion of the central β-sheet consisting of strands β7, β10, β11 and β4 forms the side of the cleft. The cap′ of the opposite subunit forms the roof. The conformation of the cap′/α2 interface does not change significantly on refinement of the T state AMP complex, despite the indications of the difference electron density map. A small change in position of the side-chain of Asn44′ accompanied by a main-chain shift is observed. The most significant conformational change is that of Arg309, whose side-chain NH-1 and NH-2 shift between 5 and 6 Å in order to contact the phosphate group of AMP. The conformation of AMP is described in Table 5. The glycosidic bond is *anti* and the ribose C-3′ is *endo*. There is an unusual conformation about C-4′–C-5′ that differs from the single crystal structure of AMP (Kraut & Jensen, 1963) and the conformation of other nucleotides (Sundaralingham, 1975). Two separate refinements of the GP*b*–AMP complex resulted in similar values for the C-4′–C-5′ torsion angle. Both refinements started with the AMP in the single crystal structure conformation: in one, the force constant on the torsion angle was low (1·5 kcal mol^{-1} deg^{-1}) and in the other the force constant was raised to 50 kcal mol^{-1} deg^{-1}. Examination of the omit map in which the phases had been computed from the protein atoms alone showed electron density that corresponded well with the conformation achieved by the refinement (Fig. 4(b)). Thus, although the conformation for the C-4′–C-5′ bond is unusual, it is supported by the experimental evidence. Relatively few specific contacts are formed between AMP and the enzyme, consistent with the observation that AMP is bound with a low level of affinity by T state GP*b*. The interactions made consist of salt-bridges between the side-chains of Arg309 and Arg310 of α8 to the phosphate group of AMP. A hydrophobic interaction is produced between the side-chain of Tyr75 of α2, stacking co-planar with the adenine base with the closest contact 3·5 Å. The closest contacts between the side-chain atoms of Asn44′ and the N-1 and N-3 atoms of the adenine base are too long (5·1 Å and 3·7 Å, respectively) for hydrogen bonds and the density for Asn44′ is weak. There is a hydrogen bond of N-3 through water to Gln72. Details of the interactions are given in Table 6 and the structure is shown in Figure 10(b).

At the nucleoside inhibitor site, the adenine

Table 5
Conformations of AMP

Torsion angle	R state GP*b*–AMP complex	T state GP*a*–AMP complex		Single crystal structure (Kraut & Jensen, 1963)
	Site N allosteric site	Site N allosteric site	Site I inhibitor site	
$O_{(4')}$–$C_{(1')}$–$N_{(9)}$–$C_{(8)}(\chi)$	33	32	47	26
$C_{(3')}$–$C_{(4')}$–$C_{(5')}$–$O_{(5')}(\psi)$	55	−17	54	40
$C_{(4')}$–$C_{(5')}$–$O_{(5')}$–$P(\phi)$	−168	−164	−92	177
Ribose	C-3′ *endo*	C-3′ *endo*	C-3′ *endo*	C-3′ *endo*

moiety is sandwiched between the planar side-chains of Phe285 and Tyr613. A water-mediated hydrogen bond occurs between the N-6 amino group and main-chain N and O atoms of Asp283. The ribose and phosphate groups project into solvent and density extends only partially over the ribose, with weak density corresponding to the phosphate group, implying that these groups are mobile. In the conformation resulting from the refinement, the phosphate group forms a hydrogen bond to the side-chain of Asn282 and to main-chain O of Pro611. No conformational change at the inhibitor or neighbouring catalytic site is observed. On binding to the inhibitor site, nucleosides and nucleotides at high concentration stabilize the T state conformation of the 280s loop, maintaining the catalytic site and tower helix in the T state conformation.

(ii) *R state AMP complex*

The global tertiary and quaternary structures of the R state GP*b*–AMP complex are identical to those of unliganded R state GP*a* and GP*b*, except for small shifts in the cap residues. The conformation of AMP bound (Table 5) is similar to the single crystal structure (Kraut & Jensen, 1963) and is supported by the electron density (Fig. 4(a)). In the R state, disordering of residues 282 to 286 (the 280s loop) abolishes the inhibitor site and AMP is not observed at this location.

A high-affinity AMP-binding site is created in R state GP following the conformational changes produced by phosphorylation or by sulphate binding to the Ser-P site. The interior of the allosteric site cleft becomes more tightly packed following the motion of the cap′ and the binding of AMP within. The R state structure exhibits complementarity with the AMP in the side-chain positions of residues from the cap′ and α2 and α8. These contacts are shown in Table 6 and Figure 10(a).

For comparison of the positions of AMP bound to T state GP*b* and R state GP*b*, we use the interface between the C termini of the α2 and α8 helices as the reference point, as these superimpose closely between the T and R states. On transition from the T state to R state, AMP is displaced towards the interior of the cleft by 2 Å and the ligand is rotated (Fig. 10(c)). The displacement moves the phosphate group of AMP towards the positively charged cluster of side-chains Arg242 of β11 and Arg309 and 310 of the α8 helix. The geometry of the salt-bridges between the phosphate group and guanidinium groups of Arg309 and Arg310 is improved. The distance between Arg242 and the phosphate group is shortened from 5 Å in the T state complex to 4 Å in the R state. The displacement of AMP requires that the side-chain of Tyr75 of α2 rotate by 70° about C^{α}–C^{β}, turning in towards the cleft, in order to stack co-planar with the adenine base. In this position, the OH group of Tyr75 forms a hydrogen bond to the AMP phosphate group.

Table 6
Interactions between AMP and protein

A. *R state GP*b*–AMP complex*	
Salt-bridges and H bonds <3·5 Å	
O-1P AMP	Arg309 NH1
O-1P AMP	Arg310 NE
O-1P AMP	Arg310 NH1
O-3P AMP	Arg309 NH1
O-1P AMP	Tyr75 OH
O-3P AMP	Tyr75 OH
O-2′ AMP	Asp42′ OD1
N-1 AMP	Asn44′ ND2
van der Waals' <4·0 Å	
Ribose	Val45′, Gln71, Tyr75
Adenine	Asn44′, Gln72, Tyr75
Contacts are listed if they feature in 2 or more subunits	
B. *T state GP*b*–AMP complex*	
Allosteric site	
Salt-bridges and H bonds <3·5 Å	
O-1P AMP	Arg310 NE
O-1P AMP	Arg310 NH1
O-2P AMP	Arg309 NH1
O-3P AMP	Arg309 NH1
van der Waals' <4·0 Å	
Ribose	Gln72, Tyr75
Adenine	Asn44′, Gln72, Tyr75
Inhibitor site	
Salt-bridges and H bonds <3·5 Å	
O-1P AMP	Pro611 O
O-2P AMP	Asn282 ND2
N-6 AMP . . .WAT.	Asp283 N
van der Waals' 4·0 Å	
Phosphate	Asn282, Glu287, Pro611, Gly612
Ribose	Phe285, Glu287, Gly612
Adenine	Asn282, Phe285, Asn613

Table 7
Solvent accessibility calculations

	R state GP*b*		T state GP*b*			
	Allosteric site		Allosteric site		Inhibitor site	
	Area buried (Å^2)	Area buried (%)	Area buried (Å^2)	Area buried (%)	Area buried (Å^2)	Area buried (%)
Phosphate	106	95	103	80	69	66
Ribose	158	98	124	80	54	32
Adenine	175	88	97	47	167	85
Total	440	93	324	66	289	62

Residues of the cap′ form interactions with the ribose and adenine moiety of AMP in the R state but not in the T state. These contacts are optimized following a motion of residues 40′ to 45′ by 0·75 Å on AMP binding relative to that of unliganded R state GP towards AMP and the α2 helix. Val45′ is in van der Waals' contact with the non-polar face of the ribose sugar. A hydrogen bond is made between the N-1 atom of an adenine ring with the side-chain of Asn44′ of the cap′, and the side-chain of Asp42′ of the cap′ forms a hydrogen bond to 2′ OH of the ribose. (In the 2′ *endo* conformation of the ribose, this contact is too close.) Further stabilization of AMP binding is achieved through the packing of the side-chains of Gln71 and Tyr75 of the α2 helix against the ribose ring.

The more extensive burial of AMP by R state GP compared to T state GP is evident from the increase in solvent area made inaccessible upon binding of AMP to the enzyme. Some 93% of solvent-accessible area (440 Å^2) is buried following binding of AMP to R state compared to 66% (324 Å^2) of solvent-accessible area buried on binding to T state (Table 7).

Further support for the notion that AMP possesses the correct structure to interact favourably with residues of the allosteric site of the R state rather than the T state is provided by examination of the phosphate-binding site. In the T state, the specificity of AMP binding is dominated by the phosphate moiety, a feature that is exploited by other phosphorylated ligands (e.g. phosphate, ATP, ADP, Glc 1-P, UDPG (Lorek *et al.*, 1984; Oikonomakos *et al.*, 1988)) that also bind to T state GP*b* with their phosphate groups interacting with Arg309 and Arg310. However, the site occupied by inorganic phosphate bound to T state GP*b* is displaced 2 Å towards Arg242 from the phosphate group of AMP. In contrast, the sulphate-binding site on R state GP*a* superimposes more closely to the phosphate group of AMP bound to R state GP*b*. Thus, in the R state, the AMP phosphate occupies a favourable dianion-binding site but in the T state, the AMP phosphate group occupies a site that is displaced from the high-affinity site. In the T state, the rather meagre contacts made between enzyme and the base and ribose of AMP and the recognition that the phosphate group does not reach the high-affinity site indicate a site that is poorly tailored to fit AMP.

4. Discussion

Protein phosphorylation promotes a change in the quaternary and tertiary conformation of glycogen phosphorylase. The close coupling between these two effects leads to a change in the subunit interface and underlies the mechanism of signal transmission to sites remote from that of phosphorylation. The N-terminal residues 10 to 21 undergo a substantial tertiary conformational change and become more ordered. The Ser14-P interacts with residues Arg69 and Arg43′, both of which shift in order to interact with the phosphate group. Formation of a high-affinity AMP site is achieved through a change in the association of the cap′ relative to the α2 and α8 helices of the opposite subunit. Since this closer association is brought about by a concerted quaternary and tertiary conformational change, both allosteric sites are altered simultaneously. Almost all the changes required to create the high-affinity AMP site are accomplished on the transition from T state GP*b* to R state GP*b*, and very few further changes are observed on binding of AMP to the R state. Transmission of the signal to the catalytic site is achieved by a change in the packing geometry of the pair of tower helices promoted by the quaternary conformational change. Each tower helix links the subunit interface to the catalytic site and a tilt of the helix on conversion to the R state causes disordering of the 280s loop and movement of Arg569 into the catalytic site. A more detailed description of the events at the catalytic site is given in the account of the sulphate activation of GP*b* (Barford & Johnson, 1989).

R state GP*a* and ammonium sulphate-activated GP*b* are structurally nearly identical, and this is consistent with kinetic, ultracentrifuge and electron spin resonance measurements on the effect of ammonium sulphate on GP*b* in solution. These studies showed that ammonium sulphate induces GP*a*-like properties in GP*b*, such as AMP-independent activation of the enzyme, enhanced AMP affinity, reversal of glucose 6-phosphate inhibition and promotion of dimer association

into tetramers (Sotiroudis *et al.*, 1978; Leonidas *et al.*, 1990*a*). In the vicinity of the Ser-P and allosteric sites, R state GP*a*, R state GP*b* and T state GP*a* (Sprang *et al.*, 1988) are very similar and T state GP*b* is the exception. The common features of the R state allosteric site include the order/disorder transitions of the N and C-terminal tails and the concerted shifts of the subdomain α1 helix, cap, α2 helix, α4 helix and loop connecting α4 to α5. In the R state structures, the tertiary structural changes observed in the cap region are partially compensated by the quaternary changes so that several of the important subunit–subunit contacts are conserved between the T and R states (e.g. the hydrogen bonds and ionic contacts between Lys41′ and Glu195, and between main-chain O of Leu39′ and Val40′ and Arg193). Conservation of these links between the two conformational states may explain why T state GP*a* (in the presence of glucose) exhibits an R state structure at the allosteric interface and a T state structure at the tower interface. In phosphofructokinase (Schirmer & Evans, 1990), compensatory conformational changes have been noted. In this instance, the 6-F loop is required to shift. If the quaternary change took place without the shift, the subunits would clash in this region and, conversely, if the structure were to adopt a T state quaternary structure but with the loop in the R tertiary structure, there would be a gap. The combination of the tertiary and quaternary changes allow similar but not identical contacts across the subunit interface in both states of phosphofructokinase.

The key features of the stabilizing interactions of the Ser-P group are the contacts to the basic groups Arg69 and Arg43′. Comparison of T state GP*b* and R state GP*a* shows why an unphosphorylated N-terminal tail does not promote an R state structure. In the unphosphorylated form, the N-terminal tail is in an acidic environment. On phosphorylation and the substantial change in the N-terminal residues and conformational response of both arginine residues, the environment of the Ser14-P is characterized by clusters of positively charged residues. The shift of Arg43′ creates a binding site for Ile13 and Arg10, and the shift of Arg69 creates a binding site for Val15. These movements change the disposition of the cap′ relative to helix α2 and favour a change in equilibrium from T to R state. The role of the residues of the N terminus in interacting and stabilizing the R state suggests that the phosphate group, in the absence of the N-terminal residues, will not stabilize the R-state. In GP*b* activated by sulphate, the sulphate and N-terminal residues co-operate in forming the R state similar to GP*a*. Solution kinetic studies have demonstrated that sulphate is unable to activate phosphorylase *b*′, a form of phosphorylase with the N-terminal 16 residues proteolytically removed, whereas AMP-dependent activation is not altered (Leonidas *et al.*, unpublished results). Thus, the N-terminal residues function in an active role in regulating GP, not simply in the passive role of supporting Ser-P.

Comparison of the AMP-binding sites between T and R state GP*b* show different orientations of the nucleotide with respect to the enzyme and much closer association of the nucleotide and enzyme in the R state, which is characterized by an increased number of hydrogen bonds, more extensive ionic contacts of the phosphate moiety and greater accessible surface area buried. The high-affinity site is created by the changes resulting from activation either by sulphate or Ser-P, and it is remarkable how relatively small conformational changes can create such different binding modes for the same ligand to the same enzyme. The dissociation constant of AMP from T state GP*b* has been measured from calorimetric experiments to be 250 μM (Mateo *et al.*, 1984) and from fluorescence experiments to be 300 to 700 μM (Mott & Bieber, 1970). In crystals of GP*b*, where the enzyme is locked in the T state, the affinity for AMP appears lower and the allosteric site is not saturated at 2·5 mM-AMP (Johnson *et al.*, 1990). The dissociation constant for AMP from activated GP*b* is 3 μM (Buc, 1967). The structural studies described previously for T state GP*a* (Sprang *et al.*, 1987) and T state GP*b* (Sprang *et al.*, 1988) indicated different binding modes of AMP that corresponded to different orientations of the bound effector. The present work substantiates these results through a comparison of AMP binding to T state GP*b* and R state GP*b*. The refined structures reveal eight ionic contacts and hydrogen bonds (<3·5 Å) between R state GP*b* and AMP compared with four such contacts between T state GP*b* and AMP and an increase in solvent-accessible area buried of 116 $Å^2$. Chothia (1974, 1975) has calculated that approximately 25 cal mol^{-1} $Å^{-2}$ of solvent accessibility area is gained on burying groups. The difference in solvent-accessible area buried for AMP between T and R states could, on this basis, account for as much as 2·9 kcal mol^{-1} in free energy change, leading to an increase in affinity of approximately 100-fold. Thus, the increased number of polar contacts and the increased burying of AMP in the R state compared to the T state appear more than sufficient to account for the 100-fold change in affinity observed in solution experiments.

The description of the structure of AMP bound to the allosteric site is consistent with biochemical results on the ability of AMP analogues to activate phosphorylase (Okazaki *et al.*, 1968; Mott & Bieber, 1970; Morange *et al.*, 1976). These studies indicated that modification of the phosphate group abolished the ability to bind to the allosteric site, and it was subsequently shown that analogues of AMP where the phosphate group adopts only a mono-anionic charged group are also unable to activate (Withers & Madsen, 1980). AMPS, in which the 5′-phosphorothioate group is more acidic than the 5′-phosphate group of AMP, is a more powerful activator than AMP (Murray & Atkinson, 1968). The geometry of the phosphate group is important, since neither 2′-AMP or 3′-AMP are able to activate. The structural results show that in the R state the

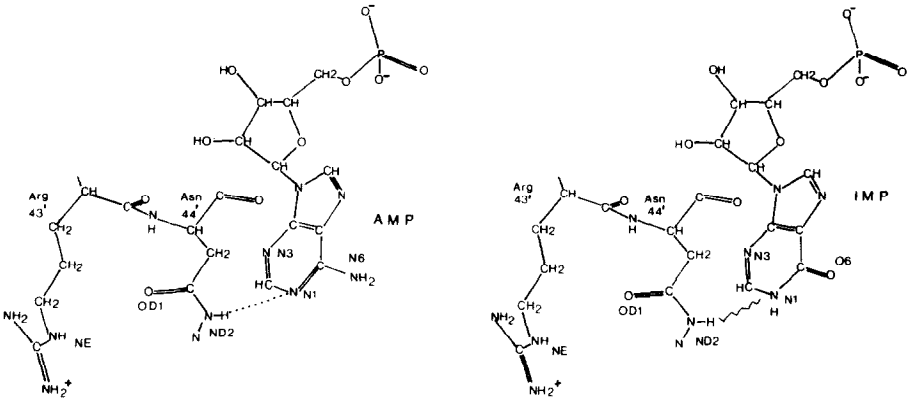

Figure 11. The observed constellation of atoms around the N-1 position of AMP in (a) the R state GP*b* complex and (b) the unfavourable juxtaposition that would arise if IMP bound in an identical manner.

phosphate recognition site is provided by direct contacts to two arginine residues (Arg309 and Arg310) and to Tyr75 with a long-range contact to Arg242. The structural results show that all three components of AMP (adenine, ribose and phosphate) make direct interactions to the protein and involve different structural elements, consistent with results that showed that neither adenosine nor ribose 5′-P activate GP*b*. The analogue 2′-deoxy-AMP has a K_d value 43-fold higher than AMP and achieves a maximal velocity only 59% that of AMP (Okasaki *et al.*, 1968). The structure shows a hydrogen bond between O-2′ and Asp42′ that is important both for binding and for subunit interactions. Conversely, 3′-deoxy-AMP is as effective as AMP in both binding and activation, and the structure shows no contact between O-3′ and the protein.

Modifications of a few groups on the adenine ring impair but do not abolish activity. It was concluded (Okasaki *et al.*, 1968) that N-3 and N-7 make relatively little contribution but that N-1 and the amino group at N-6 are important. In the T and R crystal structures, N-6 makes no direct hydrogen bonds to the protein but substitutions at this position also affect N-1. In the R state, N-1 can form a hydrogen bond to the ND2 group of Asn44′ (Fig. 10(a)). The conformation of the Asn44′ side-chain is restrained by a long (3·9 Å) contact between the OD1 atom of Asn44′ and the NE atom of Arg43′ and a bent hydrogen bond from the OD1 atom to the main-chain N of Asn44′. Although the electron density at 2·9 Å resolution does not enable the O and N atoms nor the planar orientation of the Asn side-chain to be distinguished unambiguously, nevertheless, these contacts suggest that in the R state, where the conformation of Arg43′ is constrained by its interaction with either the Ser-P or sulphate, the arginine directs the orientation of the Asn44′ side-chain such that the OD1 atom is towards Arg43′ and the ND2 atom is towards the N-1 atom of the adenine moiety of AMP. Thus, Asn44′ is a hydrogen bond donor in the interaction with N-1 (Fig. 11(a)). IMP, the deamination product of AMP in which the amino group at N-6 is replaced with a carbonyl group and N-1 is protonated, could not make this hydrogen bond (Fig. 11(b)). In principle, it should be possible for the Asn44′ side-chain to rotate so as to present the OD1 atom to hydrogen bond to the N-1-H group of IMP but this conformation would result in a less favourable grouping, in the R state, of the ND2 atom with respect to Arg43′ and the main-chain N of Asn44′. IMP is a weak activator (Cori *et al.*, 1938) that confers an increase in V_{max} without a concomitant increase in affinity for substrate (Black & Wang, 1968). Different modes of binding of AMP and IMP have been detected in measurements of transverse relaxation times in nuclear magnetic resonance experiments (Morange *et al.*, 1977). The K_d value for IMP at the allosteric activation site is 1·4 mM (Mateo *et al.*, 1984) and is considerably weaker than that for AMP (0·25 to 0·7 mM, T state; 3 μM, R state). The native T state GP*b* structure (Acharya *et al.*, 1990) was determined from crystals of the enzyme grown in the presence of 2 mM-IMP. At this concentration, the IMP was weakly bound at the allosteric and inhibitor sites. The crystal structure of the T state GP*b* with 100 mM-IMP has been studied at 2·9 Å resolution and refined by restrained crystallographic least-squares to an *R*-factor of 16% (Varvill, 1988). Comparison shows that T state AMP (100 mM) and T state IMP (100 mM) complexes are very similar, and in the T state structures there is no interaction between either N-1 or N-6/O-6 and the protein. Comparison of T state AMP or IMP complexes with R state AMP complex shows a difference in orientation and conformation (Fig. 9(a) and (b)). The different properties of AMP and IMP are also dependent on their different affinities for the allosteric site N and the inhibitor site I, as noted by others (Kasvinsky *et al.*, 1978; Uhing *et al.*, 1979; Madsen *et al.*, 1983). IMP binds with a slightly greater affinity than AMP to the inhibitor site (K_d IMP, 1·7 mM; K_{dAMP}, 3·2 mM: Mateo *et al.*, 1984). Thus, the concentration required to achieve saturation at the allosteric site with IMP results also in saturation of the inhibitor site and consequent T state stabilization of the enzyme, whereas AMP is able to achieve differential binding to the two sites and activate at concentrations that

do not saturate the inhibitor site. Thus, the only interaction that appears to differentiate between the affinity of these nucleotides at the allosteric site N is the hydrogen bond through N-1 to Asn44′ in R state AMP complexes. This appears to be a rather weak determinant for a dramatic change in kinetic properties. Site-directed mutagenesis experiments in which Asn44′ is changed to Ala could test these proposals.

Changes at the subunit interface are consistent with both the model proposed by Monod *et al.* (1965; the MWC model), and that proposed by Koshland *et al.* (1966; the KNF model) for enzyme co-operativity and regulation. In both models, the subunit interface forms the focus for transmission of information. The crucial difference between the two models is the strength of the constraints at the subunit interface. In the MWC model, effects are modulated by an equilibrium between two (or at least 2) symmetrical conformational states that differ in their affinity for ligands. A change in tertiary structure of one subunit must be accompanied by an equivalent change in the other subunits, facilitated by a quaternary conformational change, in order to conserve symmetry. In the KNF model, it was proposed that an induced tertiary conformational response to ligand binding in one subunit leads to changes in the energy of the subunit–subunit interactions that may or may not make it easier for the other subunit to respond. A sequential conformational change of subunits is envisaged in which the oligomeric assembly need not be symmetrical. Knowledge of the active and inactive structures of GP reveals nothing concerning the transient structural events occurring during the T to R transition and does not allow us to unequivocally distinguish between these models. However, certain predictions regarding the transition can be made. A complete conversion to the R state structure at one effector site at the subunit interface (e.g. Ser-P or AMP allosteric site) independent of the other allosteric site and independent of a quaternary conformational change could not occur. Creation of both sites follows from a quaternary and associated tertiary conformational changes of the cap′ that are linked to the contraction of the α2 helix and the movement of the symmetry-related cap. Hence, creation of high-affinity sites on both subunits is concerted. The positional change of the cap′ to preserve interactions with the β7 strand indicates coupling of tertiary to the quaternary structure. Moreover, constraints on the geometry of the tower helix prevents formation of intermediate structures, ensuring that the tertiary structural change of the tower is strictly coupled to the quaternary conformational change. Examination of the model suggests that the T to R conformational change at the allosteric site is an obligatory response to Ser14 phosphorylation; i.e. the cap′/α2 interface is changed concomitantly with the localization of the N-terminal tail and the binding of the Ser-P. Activation by AMP must also lead to a similar constellation at the cap′/α2 interface in order to generate a high-affinity AMP site but probably does not require ordering of the N-terminal tail. Indeed, ordering of the N-terminal tail without phosphorylation would result in unfavourable proximity of basic groups. Although we do not have a structure of R state GP*b* without the ordered tail, this hypothesis is supported by the results of cross-linking experiments (Gusev *et al.*, 1979) in which it was shown that additional cross-links that involve the N-terminal tail are observed in GP*a* but not in AMP-activated GP*b*.

To date, there are two phospho-regulated enzymes whose detailed structures are known, glycogen phosphorylase and isocitrate dehydrogenase. Their regulatory mechanisms are different. The structural mechanism of phosphorylase is similar to that of allosteric regulation: the phosphorylated N-terminal tail acts as an allosteric effector that binds to its recognition site and favours conformational changes that affect sites remote from the phosphorylation site. The bacterial enzyme, isocitrate dehydrogenase, is regulated by phosphorylation on Ser113 leading to inhibition of the enzyme, a property that can be mimicked by site-directed mutants such as Ser113Asp (Thorsness & Koshland, 1987). The crystallographic studies (Hurley *et al.*, 1990*a*,*b*) have shown that Ser113 is located close to the isocitrate-binding site and there is no substantial change in conformation between the phosphorylated and non-phosphorylated forms of the enzyme. The crystallographic and kinetic studies (Dean & Koshland, 1990) support the notion that inhibition is achieved through direct electrostatic interaction at the ligand-binding site. Thus, as Hurley *et al.* (1990*b*) suggest, regulatory covalent modification may act by two alternative mechanisms, modification at an allosteric site or direct interaction of a covalently modified amino acid with ligand binding. There is preliminary evidence for one or other of these mechanisms in other phospho-regulated proteins (although additional mechanisms may be discovered). In $p34^{cdc2}$ protein kinase, inhibition results from phosphorylation of a tyrosine residue that is part of the putative ATP-binding site (Gould & Nurse, 1989). In HPr, a component of the bacterial phosphoenolpyruvate-dependent sugar transport system, nuclear magnetic resonance structural studies indicate that the site of phosphorylation (Ser46) is remote from the catalytic histidine residue (His15), and there are substantial changes in the proton chemical shifts between the phosphorylated and non-phosphorylated forms of the protein (Wittekind *et al.*, 1989). Curiously, different mechanisms operate in the two isozymes of fructose 6-phosphate 2-kinase/fructose-2,6-bisphosphatase. In the liver isoform, the kinase activity is inhibited by phosphorylation by protein kinase A at a serine residue (Ser32) that is not too far in sequence from residues that are part of the putative nucleotide-binding site (Lively *et al.*, 1988). In the heart isoform, which is closely similar to the liver enzyme in regions of the nucleotide and substrate-binding site, phosphorylation by protein kinase A activates the

enzyme and the sites of phosphorylation have been shown to be located close to the C terminus of the protein, remote in sequence from the ligand-binding sites (Sakata & Uyeda, 1990).

Comparison of the R and T states of GP give few clues as to how phosphorylase is recognized by phosphorylase kinase and phosphorylase phosphatase. The activities of both modifying enzymes are sensitive to the conformation of their substrates. Phosphorylase kinase exhibits a lower K_m and higher V_{max} for phosphorylase than for synthetic oligopeptides, although it is an efficient catalyst for the latter substrates (Tessmer *et al.*, 1977). Protein phosphatase 1G is sensitive to ligand binding to phosphorylase and, in general, the ligands that promote the T state activate the enzyme and the ligands that promote the R state inhibit (Martensen *et al.*, 1973; Detwiler *et al.*, 1977; for a review, see Madsen, 1986). The acidic environment of Ser14 in T state GP*b* suggests that this may not be the environment in which the kinase-catalysed phosphorylation takes place. The recognition properties of these enzymes involved in control by reversible phosphorylation are problems for the future.

The co-ordinates for the phosphorylase structures have been deposited in the Protein Data Base (Bernstein *et al.*, 1977: access numbers 1GPA (R state GP*a*), 7GPB (R state GP*b*–AMP) and 8GPB (T state GP*b*–AMP).

This work has been supported by the Medical Research Council. We thank the staff at the Synchrotron Radiation Source, Daresbury, and Dr G. L. Taylor and Dr E. F. Garman for management of our Laboratory computing and area detector facilities, respectively. We are grateful to our colleagues Dr K. R. Acharya, J. L. Martin and N. G. Oikonomakos for assistance and useful discussions. L.N.J. is a member of the Oxford Centre of Molecular Sciences, which is supported by the SERC and MRC. S.-H.H. has been supported by the British Council and the Government of China.

References

Acharya, K. R., Stuart, D. I., Varvill, K. M. & Johnson, L. N. (1990). *Glycogen Phosphorylase* b. World Scientific Publishers, in the press.

Arndt, U. W. & Wonacott, A. J. (1977). *The Rotation Method in Crystallography*, North Holland, Amsterdam.

Barford, D. & Johnson, L. N. (1989). *Nature (London)*, **340**, 609–616.

Bernstein, F. C., Koetzle, T. F., Williams, G. J. B., Meyer, E. F., Brice, M. D., Rodgers, J. R., Kennard, O., Shimanouchi, T. & Tusumi, M. (1977). *J. Mol. Biol.* **112**, 535–542.

Black, W. J. & Wang, J. H. (1968). *J. Biol. Chem.* **243**, 5892–5898.

Brunger, A. T. (1989). *Acta Crystallogr. sect. A*, **45**, 42–50.

Brunger, A. T., Karplus, M. & Petsko, G. A. (1989). *Acta Crystallogr. sect. A*, **45**, 50–61.

Buc, H. (1967). *Biochem. Biophys. Res. Commun.* **28**, 59–64.

Busby, S. J. W. & Radda, G. K. (1976). *Curr. Topics Cell Regul.* **10**, 89–160.

Carson, M. & Bugg, C. E. (1986). *J. Mol. Graph.* **4**, 121–122.

Chothia, C. (1974). *Nature (London)*, **248**, 338–339.

Chothia, C. (1975). *Nature (London)*, **254**, 304–308.

Cohen, P. (1988). *Proc. Roy. Soc. ser. B*, **234**, 115–144.

Cori, G. T., Colowick, S. P. & Cori, C. F. (1938). *J. Biol. Chem.* **123**, 381–389.

Dean, A. M. & Koshland, D. E. (1990). *Science*, **249**, 1044–1046.

Detwiler, T. C., Gratecos, D. & Fischer, E. H. (1977). *Biochemistry*, **3**, 4818–4823.

Engers, H. D. & Madsen, N. B. (1968). *Biochem. Biophys. Res. Commun.* **97**, 513–519.

Fasold, H., Ortlandel, F., Huber, R., Bartels, K. & Schwager, P. (1972). *FEBS Letters* **21**, 229–232.

Fischer, E. H. & Krebs, E. G. (1962). *Methods Enzymol.* **5**, 369–372.

Fletterick, R. J., Sygusch, J., Murray, N., Madsen, N. B. & Johnson, L. N. (1976). *J. Mol. Biol.* **103**, 1–13.

French, G. S. & Wilson, K. S. (1978). *Acta Crystallogr. sect. A*, **34**, 517–525.

Gould, K. L. & Nurse, P. (1989). *Nature (London)*, **342**, 39–45.

Graves, D. J. & Wang, J. H. (1972). In *The Enzymes* (Boyer, P. D., ed.), 3rd edit., vol. 7, pp. 435–482, Academic Press, New York.

Gusev, N. B., Hajdu, J. & Friedrich, P. (1979). *Biochem. Biophys. Res. Commun.* **90**, 70–77.

Helmreich, E. & Cori, C. F. (1964). *Proc. Nat. Acad. Sci., U.S.A.* **51**, 131–138.

Howard, A. J., Gilliland, G. L., Finzel, B. C., Poulous, T. L., Oklendorf, D. H. & Salemme, F. R. (1987). *J. Appl. Crystallogr.* **20**, 383–387.

Huang, C. Y. & Graves, D. J. (1970). *Biochemistry*, **9**, 660–671.

Hurley, J. H., Dean, A. M., Thorsness, P. E., Koshland, D. E. & Stroud, R. M. (1990*a*). *J. Biol. Chem.* **265**, 3599–3602.

Hurley, J. H., Dean, A. M., Sohl, J. L., Koshland, D. E. & Stroud, R. M. (1990*b*). *Science*, **249**, 1012–1016.

Johnson, L. N. & Barford, D. (1990). *J. Biol. Chem.* **265**, 2409–2412.

Johnson, L. N., Madsen, N. B., Mosley, J. & Wilson, K. S. (1974). *J. Mol. Biol.* **90**, 703–717.

Johnson, L. N., Hajdu, J., Acharya, K. R., Stuart, D. I., McLaughlin, P. J., Oikonomakos, N. G. & Barford, D. (1989). In *Allosteric Enzymes* (Herve, G., ed.), pp. 81–127, CRC Press, Boca Raton, FA.

Johnson, L. N., Acharya, K. R., Jordan, M. D. & McLaughlin, P. J. (1990). *J. Mol. Biol.* **211**, 645–661.

Jones, A. T. (1978). *J. Appl. Crystallogr.* **11**, 272–288.

Kabsch, W. (1978). *Acta Crystallogr. sect. A*, **34**, 827–828.

Kabsch, W. (1988). *J. Appl. Crystallogr.* **21**, 67–71.

Kasvinsky, P. J., Madsen, N. B., Sygusch, J. & Fletterick, R. J. (1978). *J. Biol. Chem.* **253**, 3343–3351.

Koshland, D. E., Nemethy, G. & Filmer, D. (1966). *Biochemistry*, **5**, 365–385.

Kraut, J. & Jensen, L. H. (1963). *Acta Crystallogr.* **16**, 79–88.

Krebs, E. G. (1986). In *The Enzymes* (Boyer, P. D. & Krebs, E. G., eds), 3rd edit., vol. 17, pp. 3–20, Academic Press, New York.

Krebs, E. G. & Fischer, E. H. (1956). *Biochim. Biophys. Acta* **20**, 150–157.

Lee, B. & Richards, F. M. (1971). *J. Mol. Biol.* **55**, 379–400.

Leonidas, D. D., Oikonomakos, N. G., Papageorgiou, A. C., Xenakis, A., Cazianis, C. T. & Bem, F. (1990). *FEBS Letters*, **261**, 23–27.

Lively, M. O., El-Maghrabi, M. R., Pilkis, J., D'Angelo, G., Colosia, A. D., Ciavola, J. A., Fraser, B. A. & Pilkis, S. J. (1988). *J. Biol. Chem.* **263**, 839–849.

Lorek, A., Wilson, K. S., Sansom, M. S. P., Stuart, D. I., Stura, E. A., Jenkins, J. A., Zanotti, G., Hajdu, J. & Johnson, L. N. (1984). *Biochem. J.* **218**, 45–60.

Madsen, N. B. (1986). In *The Enzymes* (Boyer, P. D. & Krebs, E. G., eds), 3rd edit., vol. 17, pp. 366–394, Academic Press, New York.

Madsen, N. B., Honikel, K. O. & James, M. N. G. (1972). In *Metabolic Interconversion of Enzymes* (Wieland, O., Helmreich, E. & Holzer, H., eds), p. 448, Springer, Berlin.

Madsen, N. B., Shechosky, S. & Fletterick, R. J. (1983). *Biochemistry*, **22**, 4460–4465.

Martensen, T. M., Brotherton, J. E. & Graves, D. M. (1973). *J. Biol. Chem.* **248**, 8329–8336.

Martin, J. L., Johnson, L. N. & Withers, S. G. (1990). *Biochemistry*, **29**, 10745–10757.

Mateo, P. L., Baron, C., Obdulio, L. M., Jimenez, J. S. & Cortijo, M. (1984). *J. Biol. Chem.* **259**, 9384–9389.

Metzger, B. E., Helmreich, E. & Glaser, L. (1967). *Proc. Nat. Acad. Sci., U.S.A.* **51**, 131–138.

Meyer, F., Heilmeyer, L. M. G., Hashke, R. H. & Fischer, E. H. (1970). *J. Biol. Chem.* **245**, 6642–6648.

Monod, J., Wyman, J. & Changeux, J.-P. (1965). *J. Mol. Biol.* **12**, 88–118.

Morange, M., Garcia Blanco, F., Vandenbunder, B. & Buc, H. (1976). *Eur. J. Biochem.* **65**, 53–563.

Morange, M., Kolb, A. & Buc, H. (1977). *Eur. J. Biochem.* **74**, 99–106.

Mott, D. M. & Bieber, A. L. (1970). *J. Biol. Chem.* **245**, 4058–4066.

Murray, A. W. & Atkinson, M. R. (1968). *Biochemistry*, **7**, 4023–4029.

Nybourg, J. & Wonacott, A. J. (1977). In *The Rotation Method in Crystallography* (Arndt, U. W. & Wonacott, A. J., eds), pp. 139–152, North-Holland, Amsterdam.

Oikonomakos, N. G., Acharya, K. R., Stuart, D. I., Melpidou, A. E., McLaughlin, P. J. & Johnson, L. N. (1988). *Eur. J. Biochem.* **173**, 569–578.

Okazaki, T., Nakazana, A. & Hagaish, O. (1968). *J. Biol. Chem.* **243**, 5266–5271.

Rayment, I. (1983). *Acta Crystallogr. sect. A*, **39**, 102–116.

Sakata, J. & Uyeda, K. (1990). *Proc. Nat. Acad. Sci., U.S.A.* **87**, 4951–4955.

Schirmer, T. & Evans, P. R. (1990). *Nature (London)*, **343**, 140–145.

Schulz, G. E. & Schirmer, R. H. (1979). *Principles of Protein Structure*, Springer Verlag, New York.

Sotiroudis, T. G., Oikonomakos, N. G. & Evangelopoulos, A. E. (1978). *Biochem. Biophys. Res. Commun.* **90**, 234–239.

Sprang, S. R. & Fletterick, R. J. (1979). *J. Mol. Biol.* **131**, 523–551.

Sprang, S. R., Goldsmith, E. J. & Fletterick, R. J. (1987). *Science*, **237**, 1012–1019.

Sprang, S. R., Acharya, K. R., Goldsmith, E. J., Stuart, D. I., Varvill, K., Fletterick, R. J., Madsen, N. B. & Johnson, L. N. (1988). *Nature (London)*, **336**, 215–221.

Stock, J. B., Stock, A. M. & Mottonen, J. M. (1990). *Nature (London)*, **344**, 395–400.

Sundaralingham, M. (1975). In *Structure and Conformation of Nucleic Acids* (Sundaralingham, M. & Rao, S. T., eds), pp. 487–523, University Park Press, Baltimore.

Tessmer, G. W., Skuster, J. R., Tabatabai, L. B. & Graves, D. J. (1977). *J. Biol. Chem.* **252**, 5666–5671.

Thorsness, P. E. & Koshland, D. E. (1987). *J. Biol. Chem.* **262**, 10422–10425.

Uhing, R. J., Janski, A. M. & Graves, D. J. (1979). *J. Biol. Chem.* **254**, 3166–3169.

Varvill, K. M. (1988). D.Phil. thesis, University of Oxford.

Wang, J. H., Shonka, M. L. & Graves, D. J. (1965). *Biochemistry*, **4**, 2296–2301.

Wansom, J.-C. & Drochmans, P. J. (1968). *J. Cell. Biol.* **38**, 130–150.

Weiss, W. I., Brunger, A. T., Skehel, J. J. & Wiley, D. C. (1990). *J. Mol. Biol.* **212**, 73–761.

Withers, S. G. & Madsen, N. B. (1980). *Biochem. Biophys. Res. Commun.* **33**, 49–54.

Wittekind, M., Reizer, J., Deutscher, J., Saier, M. H. & Klevitt, R. E. (1989). *Biochemistry*, **28**, 9908–9912.

Yarden, Y. & Ullrich, A. (1988). *Annu. Rev. Biochem.* **57**, 443–478.

Edited by A. Klug